STRONGLY CORRELATED QUANTUM MATTER: A SUBJECTIVE OVERVIEW OF SELECTED FUNDAMENTAL ASPECTS*

Józef Spałek

Institute of Theoretical Physics, Jagiellonian University
Łojasiewicza 11, 30-348 Kraków, Poland

(Received May 5, 2020)

In this brief overview, I address some of the fundamental topics related to the physics of strongly correlated fermions, which have been also the subject of my research. After addressing the question why the field has a fundamental meaning, we next turn to the specific problems with their simple theoretical description. Those topics are: *(i)* the concept of spin-dependent masses of heavy particles and its subsequent experimental verification; *(ii)* the correlated metal–insulator transitions of the Mott–Hubbard-type; *(iii)* real space pairing and its subsequent experimental verification for high-temperature superconducting cuprates. I mention also the persistence of quantum spin and charge excitations in the superconducting phase. All those phenomena confirm the view that the strongly correlated fermionic systems represent a new class of *quantum liquids*, with some properties quantitatively different than those of the Landau Fermi liquids. Namely, they can be classified as those that fall in between those of the anomalous Landau Fermi liquid and localized-magnetic-moment system.

DOI:10.5506/APhysPolB.51.1147

1. Introduction: Fundamental features of correlated systems

The fundamental theoretical work on correlated fermion systems started with intuitive considerations by Mott and Anderson, and was formally reformulated by Hubbard (*cf.* the summaries of an early-stage effort in Refs. [1–3] respectively). The main overall features of the nonrelativistic correlated systems can be briefly characterized as follows.

* Based on the plenary talk presented at the 45$^{\text{th}}$ Congress of Polish Physicists, Kraków, September 13–18, 2019, on the occasion of receiving the Marian Smoluchowski Medal in Physics.

1.1. Definitions

The ground-state energy of a periodic condensed system of fermions can be described by starting from the system atomic configuration and, subsequently, adding other dynamic interactions which appear in the emerging condensed state. Namely, its energy per atomic state can be expressed in the form of [4]

$$\frac{E_{\mathrm{G}}}{N} = \epsilon_a + \langle T\rangle + \langle V\rangle + \langle V_{12}\rangle \equiv E_1 + E_2\,, \tag{1}$$

where ϵ_a is the single particle in an atomic (Wannier) state, $\langle T\rangle$ and $\langle V\rangle$ are the average kinetic and potential energies in the state, whereas $\langle V_{12}\rangle$ is the expectation value of the two-particle interaction. Thus, the single-particle part E_1 comprises the first three terms and $E_2 \equiv \langle V_{12}\rangle$. In such a periodic system near the delocalization–localization transition, we usually assume that $\epsilon_a = 0$, *i.e.*, it acquires a constant (reference) value which is often disregarded unless stated explicitly. In this manner, the remaining terms characterize solely the contributions of relevant fermions in condensed state. Note also that usually $E_1 < 0$. Next, one can define two physically distinct regimes:

1. $|E_1| \gtrsim E_2$: Fermi-liquid (metallic) regime, ranging to the delocalization–localization threshold when $|E_1| \approx E_2$;
2. $|E_1| \ll E_2$: Strong-correlation (Mott) regime.

Let us characterize briefly each of them and introduce the states in these regimes. Connected with this is the start from *atomic* (Wannier) representation of the involved states and interactions, although in situation 1. the starting point is often described by either gas of fermions or the Landau Fermi liquid and associated with them momentum representation and the Fermi–Dirac statistics in its canonical form. In discussing the correlated systems, we start as a rule from the Wannier representation (see below). This means that we start from two complementary representations of the quantum-mechanical states, *i.e.*, in the Bloch representation the momentum uncertainty is zero, whereas in the Wannier representation, the proper quantum number is the fixed lattice position at which the wave function is centered.

1.2. Mott–Hubbard localization–delocalization transition

The above division into the asymptotic regimes is illustrated in Fig. 1, where the *complementary* nature of the single-particle states is represented on an example of a solid with metallic (delocalized) states of electrons (a)

or correlated (atomic, Mott) states (b) for the case with one relevant valence electron per parent atom. Additionally, we have marked the dividing line (Mott–Hubbard boundary) between the two macrostates. An important remark should be provided already here. First, the momentum representation is described by the Bloch functions $\{\Psi_{\boldsymbol{p}\sigma}(\boldsymbol{r})\}$ of particle with (quasi)momentum $\boldsymbol{p} = \hbar\boldsymbol{k}$ and the spin quantum number $\sigma = \pm 1 \equiv \uparrow, \downarrow$, whereas the position representation is expressed by the corresponding set of Wannier states $\{w_{i\sigma}(\boldsymbol{r})\}$, both in the single-band situation for fermions of spin 1/2. These two representations are equivalent in the sense that they are related by the lattice Fourier transformation. However, in the situation depicted in Fig. 1, when we have a sharp boundary (usually the first-order phase-transition line) between the states shown in (a) and (b), this equivalence is broken and, in effect, the unitary symmetry U(N) does not apply. The macroscopic state (a) near the transition is represented, strictly speaking, by a modified Landau Fermi liquid (the so-called *almost localized Fermi liquid*, ALFL), whereas the Mott-insulating state is well-accounted for as a localized-spin (Heisenberg) antiferromagnet (in the ground state).

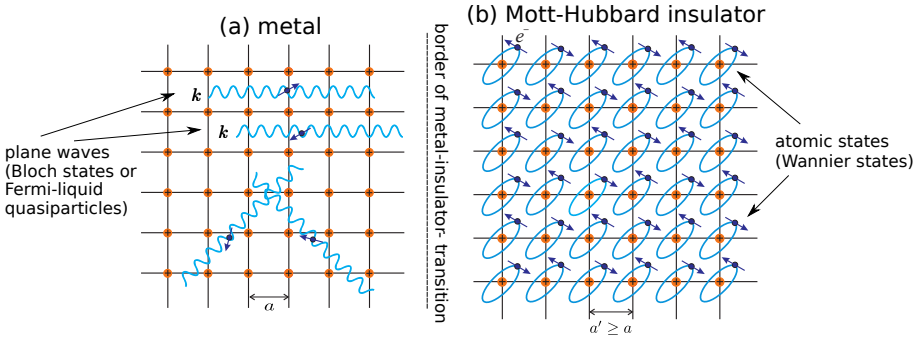

Fig. 1. Schematic representation of metallic (a) and quasiatomic (Mott-insulating) states of a planar lattice composed of hydrogen-like atoms, each with one valence electron (b). The Mott–Hubbard (metal–insulator) boundary is marked in the middle. The transition between those complementary states is as a rule *discontinuous*.

From the above qualitative picture, one can infer that with the approaching *metal* $\rightarrow$ *insulator boundary*, *i.e.*, with formation of the localized-spin state, the kinetic energy of the *renormalized-by-interaction* particle progressive motion through the system is drastically reduced and, as a result, it vanishes in the localized (insulating) state. Effectively, one can say that the Landau quasiparticle effective mass diverges, $m^* \rightarrow \infty$. This feature illustrates the situation that strong enough interactions (called in this context *strong correlations*) limit the stability of the Landau–Fermi quasiparticle picture, as is exemplified explicitly by the appearance of the Mott–Hubbard

phase transition. In addition, a proper quantitative description of the transition requires a model with a simultaneous generation of the effective exchange interactions (*kinetic exchange* [5] in the one-band case or *superexchange* in the multiple-orbital situation [5]). In the subsequent section, we provide a quantitative analysis of these statements. The starting point of these considerations is the parametrized microscopic Hamiltonian provided below.

1.3. High-temperature (high-T_c) superconductivity

Strictly speaking, *the Mott–Hubbard transition* takes place when we have one electron per relevant valence orbital (for the filling $n = 1$), *i.e.*, a half-filled band configuration when looking at it from the metallic side. The Mott insulating state appearing in such a situation is thus completely different from that of Bloch–Wilson band insulator, where the number of valence electrons per relevant orbital is $n = 2$ (even number in many-orbital situation), *i.e.*, each involved band is full (and separated from other states). This difference is exhibited explicitly by the circumstance that the Mott insulator has unpaired spins on atoms (localized states) and thus is a magnetic (usually *antiferromagnetic*) insulator, whereas the Bloch–Wilson insulator is *diamagnetic* (with zero net spin moment and magnetism solely due to the orbital moment). A fundamental question is what happens if we have holes in the Mott insulator, produced either by extrinsic doping or by self-doping. The situation is presented schematically in Fig. 2 on the example of square lattice, where we mark virtual hopping processes in the second order in the case of the Mott insulator (a) and the real hopping, in addition to

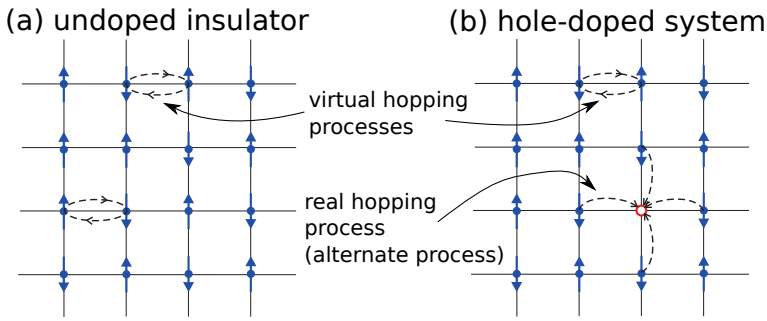

Fig. 2. Schematic representation of the particle dynamics as intersite hopping processes in real space: Virtual hopping (a) in the Mott insulating state and also real motion when holes are present (b) and, in effect, a strongly-correlated metallic state appears, for which its single-particle (band) energy is only a fraction of the corresponding short-range part of Coulomb energy.

the virtual hopping, in the situation with holes in the Mott insulator (b). It was shown first by Anderson [6, 7] that the virtual processes depicted in (a) lead to the antiferromagnetic *kinetic exchange* and, in consequence, to the *antiferromagnetic ordering* in almost all Mott insulators with odd number of electrons per atom. Those considerations have been subsequently generalized to the case of the doped insulator (correlated metal) by Spałek *et al.* [8–11] and from there the emerging later [12–14] t–J (of t–J–U) model of high-temperature superconductivity. The latter model plays a prominent role in the theory of strongly correlated systems and is discussed in the next section.

1.4. Spin-dependent masses

The interaction between correlated particles in the simplest form is taken in the form of single-band Hubbard model [3, 15]

$$\tilde{\mathcal{H}} = {\sum_{ij\sigma}}' t_{ij}\, \hat{a}^{\dagger}_{i\sigma}\, \hat{a}_{j\sigma} + U \sum_{i} \hat{n}_{i\uparrow}\, \hat{n}_{i\downarrow}\,, \tag{2}$$

in which $t_{ij} \equiv \langle w_i|\mathcal{H}_1|w_j\rangle < 0$ represents the single-particle parameter phrased as *the hopping*, with the bandwidth of bare states $W \equiv 2z|\sum_{j(i)} t_{ij}|$ and U is the magnitude of intra-atomic interactions (the so-called *Hubbard term*). For strongly correlated electrons, we can rephrase the conditions 1. and 2. as $W \lesssim U$, with $W \simeq U$ for the system at the Mott–Hubbard transition, whereas $W \ll U$ represents extreme strongly correlated limit 2. In the latter case and for $n < 1$ a specific phenomenon appears, namely the quasiparticles have spin-direction-dependent effective masses in the spin-polarized situation, *e.g.*, in a sufficiently strong applied magnetic field. This effect is large and has been predicted by us first theoretically [16, 17] and later confirmed experimentally [18]. The difference between the effective masses ($m_{\uparrow}$ and $m_{\downarrow}$) can be quite large and $m_{\uparrow} \ll m_{\downarrow}$, where the spin direction $\uparrow$ corresponds to the spin-majority quasiparticles. The situation is illustrated in Fig. 3 and the effective-mass difference can be quite large (even of an order of magnitude) [19, 20]. In Fig. 4, we display the exemplary results. The experimental results prove that the quasiparticles can be regarded in many respects as real particles.

The appearance of spin-dependent masses bears a fundamental consequence for the statistics of the correlated fermions (*e.g.*, electrons). Namely, the particles in the paramagnetic liquid state (correlated or not) are *indistinguishable* in the quantum mechanical sense. This, however, does not necessarily imply that the Fermi–Dirac distribution applies to them. On the other hand, when the masses are different: they then become *distinguishable*, particularly when their masses are different and the effective wave equations

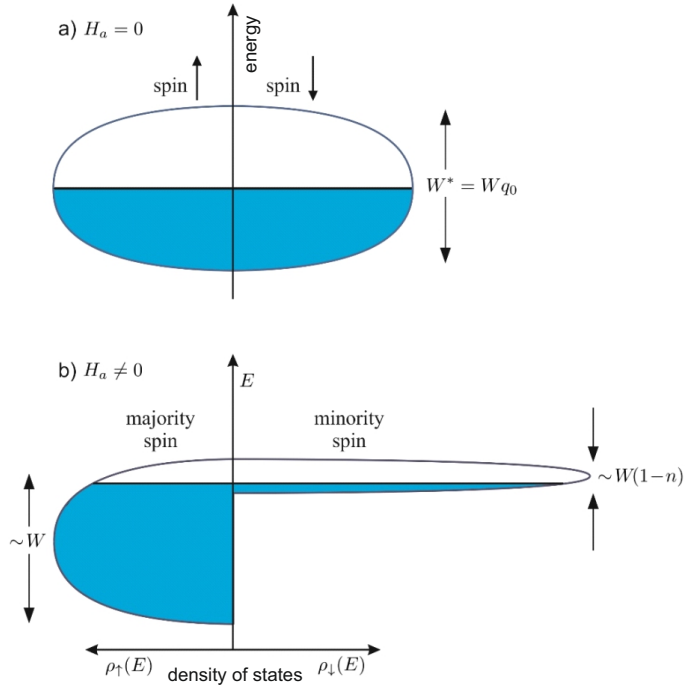

Fig. 3. Emergence of spin-dependent masses out of the paramagnetic state of correlated electrons (a), when system is polarized, *e.g.*, by applied magnetic field (b). The main source of the spin splitting are the interparticle correlations, *not the Zeeman splitting of the corresponding spin subbands.* In the saturated magnetically state, the quasiparticles acquire the bare band mass, which still may differ from free-electron mass m_0. W — bare-bandwidth and q_0 is the so-called band narrowing factor (see the next section).

for them are distinct (have different mass in the kinetic-energy term). Finally, when the system is totally spin-polarized, the minority-spin particles disappear and the only existing majority-spin (all) particles become *indistinguishable again.* Additionally, those majority-spin particles acquire in that state the bare (band) mass. This prediction, if tested experimentally, may serve as *a direct test of the question of quantum-mechanical indistinguishability versus distinguishability.* We regard this aspect of correlated states as one of the *fundamental aspects* of physics of the correlated quantum matter.

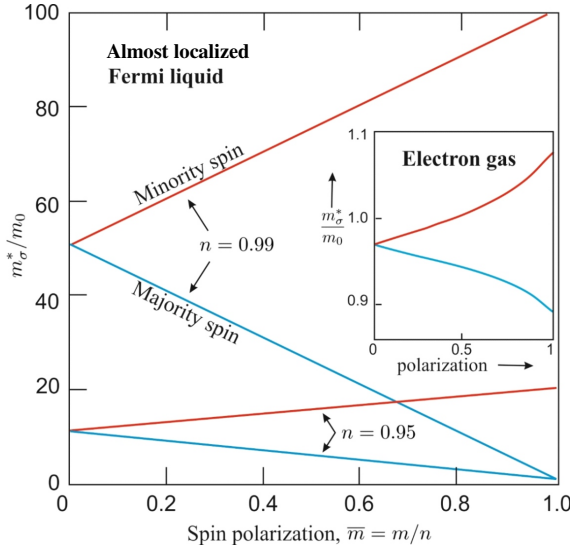

Fig. 4. Exemplary effective spin-dependent mass difference for fermions in a correlated narrow band with the band filling n close to the half filling $n = 1$ (with one valence electron per atom). Inset: the corresponding mass splitting for electron gas in an astronomically large applied field (*cf.* [21]).

2. From Landau Fermi liquid to Mott–Hubbard insulator or strongly correlated liquid

2.1. Landau Fermi-liquid theory: A brief overview

The Landau theory of Fermi liquids represents a standard reference point in the theory of interacting fermions (for recent references, see [22–24]). Here, we describe only briefly their characteristics, particularly those which appear or are included in the theory of correlated systems.

The principal assumption of the theory is that we are interested in the change of *ideal Fermi gas properties* induced by the inter-particle interactions and associated with them thermal excitations at low temperatures. In other words, we express the change of the total energy of the system due to the interaction in the form of

$$\delta E \simeq \sum_{\boldsymbol{k}\sigma} \epsilon_{\boldsymbol{k}\sigma}\, \delta n_{\boldsymbol{k}\sigma} + \frac{1}{2} \sum_{\boldsymbol{k}\boldsymbol{k}'} f^{\sigma\sigma'}_{\boldsymbol{k}\boldsymbol{k}'}\, \delta n_{\boldsymbol{k}\sigma}\, \delta n_{\boldsymbol{k}'\sigma'} \equiv \sum_{\boldsymbol{k}\sigma} E_{\boldsymbol{k}\sigma} \delta n_{\boldsymbol{k}\sigma}\,, \tag{3}$$

where $\epsilon_{\boldsymbol{k}\sigma}$ is the single-particle energy (with respect to the chemical potential terms μ) and $f^{\sigma\sigma'}_{\boldsymbol{k}\boldsymbol{k}'}$ (generally spin-dependent) is the effective interaction between those particles; it has the form of spin-dependent density–density interactions. Explicitly, $\epsilon_{\boldsymbol{k}\sigma} \equiv \epsilon_{\boldsymbol{k}} - g\mu_{\mathrm{B}} H_a \sigma - \mu$ and in the isotopic liquid

(not generally true for fermions in lattice systems), we have that $f^{\sigma\sigma'}_{\boldsymbol{k}\boldsymbol{k}'} = f^{s}_{\boldsymbol{k}\boldsymbol{k}'}(\boldsymbol{k}\cdot\boldsymbol{k}'/k_{\rm F}^2) + \sigma\sigma' f^{a}(\boldsymbol{k}\cdot\boldsymbol{k}'/k_{\rm F}^2)$, where $k_{\rm F}$ is the Fermi wave vector and $f^{s,a}$ express spin-independent and spin-dependent parts, respectively. The next assumption is that we take into account the interaction-induced scattering processes for particles at the Fermi surface, *i.e.*, put that $\frac{\boldsymbol{k}\cdot\boldsymbol{k}'}{k_{\rm F}^2} = \cos\theta_{\boldsymbol{k}\boldsymbol{k}'}$ and then we can express the interaction parameters in terms of the Legendre polynomial expansion

$$f^{(s,a)}(\cos\theta) = \sum_{l=0}^{\infty} f_l^{(s,a)} P_l(\cos\theta)\,. \tag{4}$$

There are three implicit assumptions in this formulation. First, the scattering is important only very near or, strictly speaking, at the Fermi surface due to the Pauli principle, *i.e.*, the circumstance that particles can scatter only from occupied states $|\boldsymbol{k}\sigma\rangle$ into unoccupied ones. Second, a well-defined Fermi surface exists even if the interaction is included (the Luttinger theorem proved later on the grounds of perturbation expansion and assuming validity of the Dyson theorem there; not always valid for correlated systems). The third, there is one-to-one correspondence between the initial (bare energy states, $\epsilon_{\boldsymbol{k}\sigma}$) and the effective (*quasiparticle*) states with energies $E_{\boldsymbol{k}\sigma} \equiv \epsilon_{\boldsymbol{k}\sigma} + \frac{1}{2}\sum_{\boldsymbol{k}\boldsymbol{k}'\sigma'} f^{\sigma\sigma'}_{\boldsymbol{k}\boldsymbol{k}'}\delta n_{\boldsymbol{k}'\sigma'}$. Moreover, the Fermi energy $E_{\rm F} \equiv \mu$ at $T = 0$ can be regarded as the same reference state for both *bare* and *quasiparticle* states. Effectively, this means that the interaction processes, practically active only at the Fermi surface, do not influence the Fermi surface volume. Finally, from the third assumption, it follows that the statistical distribution for the quasiparticles can be taken in the form of the Fermi–Dirac distribution for those states, *i.e.*, $f(E_{k\sigma}) = [\exp(\beta E_{k\sigma}) + 1]^{-1}$.

The ingenious feature of this theory is, in opinion of the author, that the principal properties of the Fermi liquid, such as liquid ^{3}He, can be expressed solely by the first three parameters of expansion (4): f_0^s, f_1^s, and f_0^a, what makes this theory, phenomenological in its nature, testable in its original form, at least for liquid ^{3}He. What is more, the assumption about the Fermi–Dirac distribution applicability has been tested on two systems: experimentally, for liquid ^{3}He (*cf.* Fig. 5 (a), (b)) and theoretically by considering evolution of the statistical distribution function, calculated exactly for a model nano-chains and nano-rings of hydrogen atoms, as a function of inter-atomic distance R in units of the Bohr radius a_0 (*cf.* Fig. 5 (c)) [25, 26].

Nevertheless, as shown in Fig. 5 (a), (b), the effective-mass concept (m_3^*) for the atoms breaks down and consequently, of the linear specific heat γ ceases to exist at the liquid–solid transition (*cf.* Fig. 5 (b)). Additionally, with the increasing lattice parameter R (decreasing electron density), the concept of a sharp Fermi level gradually fades away (*cf.* Fig. 5 (c)). These

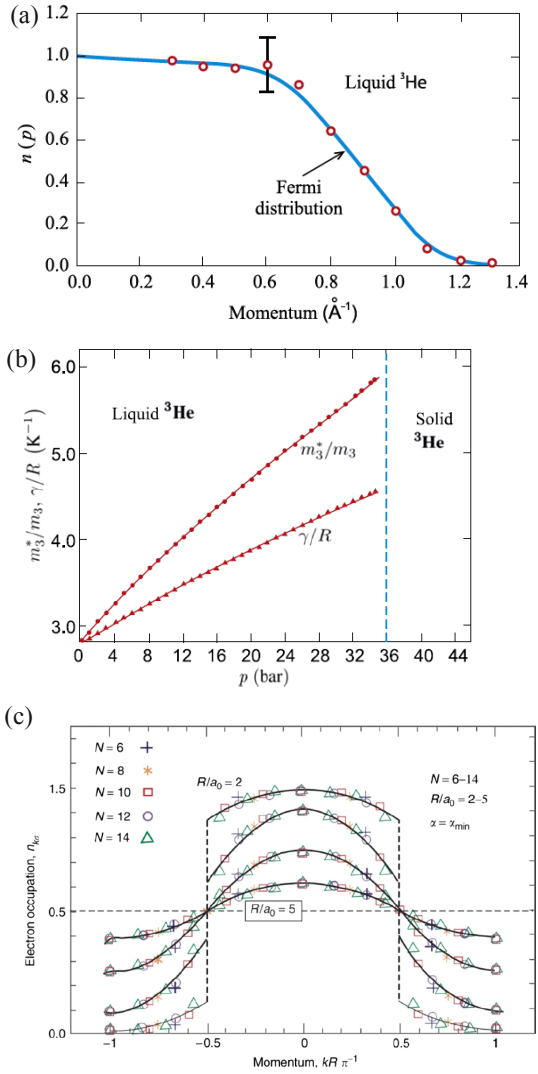

Fig. 5. Principal characteristics of liquid ^{3}He as of Fermi liquid: (a) the Fermi–Dirac distribution measured by neutron scattering [27]; (b) the linear-specific-heat coefficient γ in units of gas constant R and inferred from it effective atom mass enhancement m_3^*/m_3, both as a function of external pressure (*cf.* [28]); (c) evolution of the Fermi–Dirac distribution for linear chains composed of H atoms, with interatomic distance R (relative to Bohr radius a_0) *cf.* Refs. [25, 26].

effects cannot be accounted within the Landau Fermi-liquid theory. They are next discussed within the Hubbard model by introducing the concept of *an almost localized Fermi liquid* and a discontinuous delocalization–localization

(metal–insulator) phase transition. These aspects are regarded as the second fundamental aspects which arose from the observations in the solid state physics [4, 17, 29] (for elementary discussion of the transition, see Appendix).

2.2. An almost localized Fermi liquid (ALFL)

One can notice from Fig. 5 (b) that the Fermi-liquid state characterized there by γ/R and the effective-mass enhancement m_3^*/m_3 of the ^{3}He atom in this milieu, both loose their meaning at *the liquid–solid transition*, which takes place at the external pressure $\simeq 36$ bar. At this point the atoms freeze into well-defined crystal positions and their individual quantum mechanical state is characterized from now on by set of Wannier functions $\{w(\boldsymbol{r}\cdot\boldsymbol{R}_i)\}$ centered at well-defined lattice sites $\{\boldsymbol{R}_i\}$. It must be underlined that in this case, there is no single-particle potential trapping the particles, as it is the case of electrons in solids. Our task in this section is to briefly discuss the delocalization states on the liquid (metallic for electrons) side close to the transition to the localized state, and next, its first-order phase-transition nature. We model the system by starting from the Hubbard Hamiltonian (2) and calculate the system ground-state energy per atomic site $\langle\mathcal{H}\rangle/N$. As said above, when approaching the localization–delocalization transition, we expect that the single-particle and interaction parts become of comparable amplitude. Due to this circumstance, we assume that the hopping probability $\langle\hat{a}^\dagger_{i\sigma}\,\hat{a}_{j\sigma}\rangle$ is renormalized by the interaction to the form of $\langle\hat{a}^\dagger_{i\sigma}\,\hat{a}_{j\sigma}\rangle \equiv q\langle\hat{a}^\dagger_{i\sigma}\,\hat{a}_{j\sigma}\rangle_0$, where $\langle\hat{a}^\dagger_{i\sigma}\,\hat{a}_{j\sigma}\rangle_0$ is the hopping probability for noninteracting *(uncorrelated)* particles and q is the so-called renormalization (band narrowing) factor: $q\to 1$ when $U\to 0$ and $q\to 0$ when $U\to U_{\rm c}$, where $U_{\rm c}$ is the critical interaction value for the transition to the localized state to the take place. Explicitly, we can write down the system internal energy in the form (for $U\leqslant U_{\rm c}$) of

$$\frac{E_{\rm G}}{N}=\frac{1}{N}\sum_{\boldsymbol{k}\sigma}E_{\boldsymbol{k}}\,f(E_{\boldsymbol{k}})+Ud^2\,, \tag{5}$$

where $E_{\boldsymbol{k}}\equiv q\epsilon_{\boldsymbol{k}}$, $d^2\equiv\langle\hat{n}_{i\uparrow}\,\hat{n}_{i\downarrow}\rangle$, and $f(E_{\boldsymbol{k}})$ in the Fermi–Dirac function for renormalized particles still regarded as quasiparticles. In this function, d^2 is regarded as a variational parameter to be calculated self-consistently. Therefore, the whole problem reduces to determining microscopically $q\equiv q(d^2)$. This can be carried out by considering the Gutzwiller variational approach [30]. It turns out that for the half-filled ($n=1$) state (*i.e.*, with one particle per atomic site) and for systems with electron–hole symmetry, this factor can be calculated in the elementary manner [31] which yields in a direct manner a simple result $q(d^2)=8d^2(1-2d^2)$. Additionally, we have that for a constant density of states, the chemical potential can be set $\mu\equiv 0$

and

$$\bar{\epsilon} \equiv \frac{1}{N} \sum_{\boldsymbol{k}\sigma} (E_{\boldsymbol{k}}/q) = -\frac{W}{4}\,, \tag{6}$$

where $E_{\boldsymbol{k}}/q \equiv \epsilon_{\boldsymbol{k}}$ represents the single-particle energy of bare particles at the temperature $T = 0$ (also, effective mass renormalization is $m^* = m_{\rm B}/q$, where $m_{\rm B}$ is the bare band mass).

By minimizing energy (4) with respect to d^2, we obtain both the physical ground-state energy and the quasiparticle energy spectrum $\{E_{\boldsymbol{k}}\}$. This in turn, allows us to calculate concrete ground-state and thermodynamic properties. Explicitly [32–34],

$$\begin{cases} d^2 = \dfrac{1}{4}\left(1 - \dfrac{U}{U_{\rm c}}\right)\,, & (7) \\ \dfrac{E_{\rm G}}{N} = \dfrac{1}{4}\left(1 - \dfrac{U}{U_{\rm c}}\right)^2 \bar{\epsilon}\,, & (8) \\ \dfrac{m^*}{m_0} = \dfrac{1}{1 - \left(\frac{U}{U_{\rm c}}\right)^2} \equiv \dfrac{1}{q_0}\,, & (9) \\ \dfrac{\chi}{\gamma} = \dfrac{1 + \frac{U}{2U_{\rm c}}}{\left(1 + \frac{U}{U_{\rm c}}\right)^2}\,, & (10) \end{cases}$$

with $U_{\rm c} \equiv 8|\bar{\epsilon}| = 2W$ (the second value is for a constant density of states). Additionally, to calculate the magnetic susceptibility χ, a full Gutzwiller approach must be used [30]. When $U \to U_{\rm c} \to 0$, $d^2 \to 0$, $E_{\rm G} \to 0$, $m^* \to \infty$, and, $\chi/\gamma \to 4$. We see that at the transition, the interaction (> 0) and the single-particle (< 0) parts compensate each other, the mass for a translational motion throughout the system diverges, and the magnetic susceptibility is proportional to γ. The $U = U_{\rm c}$ point thus represents a dividing line between the itinerant and atomic states of the matter and the freezing of particle into a lattice breaks the system translational invariance (at least, in the liquid ^{3}He case). A full microscopic approach would require an explicit determination of the parameters U and $\bar{\epsilon}$ as a function of pressure. Low-temperature corrections to above (7)–(10) have been analyzed elsewhere [24, 32].

One may say that the picture formed by expressions (7)–(10) represents, as in any Fermi-liquid theory, a basic quasiparticle picture, with an additional boundary for its applicability for $U < U_{\rm c}$. In fact, this picture can be mapped into the Landau Fermi-liquid parametrization of the physical properties at $T = 0$ [35]. Such a parametrization via the renormalization factor q

in the case of ALFL is summarized in Table I. The question remains what is the collective spin- and charge-excitation spectrum in the present case. This subject is a matter of our present studies and will not be detailed here [36, 37].

TABLE I

Scaling laws of single-particle excitations in principal quantities of an almost localized Fermi liquid. The quantities are: $T^* = T/q$, $H^* = H_a/q$, $\beta^* = \beta/q$ and those with the subscript zero represent noninteracting particles, H_a is applied magnetic field, and β is the effective exchange field [40].

Property	Formula for noninteracting particles	Scaling property for ALFL
Linear specific heat	$C_V = \gamma_0 T$	$\gamma = \gamma_0/q$
Pauli paramagnetism	$M = \chi_0 H_a$	$\chi = \chi_0(T^*)/qS$
Fermi temperature	$T_{\mathrm{F}0} = \mu_0/k_{\mathrm{B}}$	$T_{\mathrm{F}} = T_{\mathrm{F}0}/q$
Density of states	$\rho(\epsilon) = \frac{1}{N}\sum_{\boldsymbol{k}} \delta(\epsilon - \epsilon_{\boldsymbol{k}})$	$\rho(E) = (1/q)\rho_0(\epsilon)$
Free energy functional	$F_0 = E_0 - TS_0$	$F(T, H_a) = q[F_0(T^*, H^*, \beta^*) + \beta^* m] + Ud^2$
Particle–particle scattering time	$\tau(\epsilon, T) = h/[(\epsilon - \mu)^2 + (k_{\mathrm{B}}T)^2]$	$\tau(\epsilon, T) = \tau_0(q, T^*)$
Quasiparticle energy	$\epsilon - \sigma H_a$	$E = q[\epsilon - \sigma(H^* - \beta^*)]$
Wilson ratio	$R_W = \chi_0/\gamma_0$	$R_{\mathrm{W}} = R_0/\tilde{S}\,, \qquad 1 < R_{\mathrm{W}} < 4$

2.3. Delocalization–localization (Mott–Hubbard) transition

As has been mentioned in the preceding section, the delocalization–localization transition at $T = 0$ takes place at $U = U_{\mathrm{c}}$. The question is when this transition will appear at arbitrary $T \geqslant 0$. This question is a nontrivial one, since near the transition, the renormalized single-particle and interaction energy not only almost compensate each other, but also each of the two terms vanish separately. In such a situation, small perturbations such as thermal or atomic disorder, or even applied magnetic field may balance the energies towards either insulating (localized) or itinerant (ALFL, metallic) state. We discuss next the effect of nonzero temperature.

Starting from the internal energy (4), we define now the free energy of the itinerant correlated system as [32, 38]

$$\frac{F}{N} = \frac{1}{N}\sum_{\boldsymbol{k}\sigma} E_{\boldsymbol{k}}\, f_{\boldsymbol{k}\sigma} + U\eta + \frac{k_{\mathrm{B}}T}{N}\sum_{\boldsymbol{k}\sigma}\left[f_{\boldsymbol{k}\sigma}\ln f_{\boldsymbol{k}\sigma} + (1-f_{\boldsymbol{k}\sigma})\ln\left(1-f_{\boldsymbol{k}\sigma}\right)\right], \tag{11}$$

where $f_{\boldsymbol{k}\sigma}$ is the Fermi–Dirac function for quasiparticles with energies $E_{\boldsymbol{k}\sigma}$ and the last term is the entropy in the given state (not necessarily the equilibrium state, which we determine by minimizing $\mathcal{F}$). This expression allows for low-temperature (Sommerfeld-type) expansion defined as the regime with $k_{\mathrm{B}}T/qW \ll 1$. In effect, the first nontrivial terms in paramagnetic state have the form of

$$\frac{F}{N} = -\Phi\frac{W}{4} + U\eta - \frac{\gamma_0 T^2}{\Phi} + O\left(T^4\right). \tag{12}$$

A detailed analysis of the low-T expansion is provided in [32], where the Gutzwiller–Brinkman–Rice approach is generalized to the $T > 0$ case in the simplest form. Note that the expressions describe the free energy functional for an almost localized Fermi liquid to be minimized with respect to d^2. As before, we assume that $\mu \equiv 0$, which means that the electron–hole symmetry holds. The next step is the introduction of discontinuous phase transition in the context of the itinerant state instability. We regard the ALFL as a well-defined phase in the thermodynamic sense and the lattice of localized electrons (spins) at the other. Then, the discontinuous phase boundary between them is determined from the coexistence condition $F = F_{\mathrm{I}}$, where F_{I} is the free energy of the insulating state and has a very simple form if the spins are disordered

$$\frac{F_{\mathrm{I}}}{N} = -k_{\mathrm{B}}T\,\ln 2\,, \tag{13}$$

where $k_{\mathrm{B}}\,\ln 2$ is the entropy of $S = 1/2$ spins. From the coexistence condition, we obtain two transition temperatures

$$k_{\mathrm{B}}T_{\pm} = \frac{3q_0}{2\pi^2}\,W\left\{\ln 2 \pm \left[(\ln 2)^2 - \frac{\pi^2}{3}\left(1-\frac{U}{U_{\mathrm{c}}}\right)^2 \Big/ q_0\right]^{1/2}\right\}. \tag{14}$$

The two solutions coalesce ($T_+ = T_- = T_{\mathrm{c}}$) for $U = U_{\mathrm{lc}}$, *i.e.*, for the lowest critical value of the interaction for the transition to take place which is determined from the condition

$$\frac{U_{\mathrm{lc}}}{U_{\mathrm{c}}} = 1 - \frac{\sqrt{3}\,\ln 2}{\pi}\,. \tag{15}$$

The corresponding critical transition temperature at $U = U_{\rm lc}$ is

$$k_{\rm B}\, T_{\rm c} = \frac{3\ln 2}{2\pi^2} W \left[1 - \left(\frac{U_{\rm lc}}{U_{\rm c}}\right)^2\right]. \tag{16}$$

For $U \leq U_{\rm lc}$, the metallic (Fermi liquid) state is stable at all T. In effect, the regime of the transition appearance is determined by conditions $U_{\rm lc} < U < U_{\rm c}$.

Disregarding the magnetic phases, one then has the following phase sequence. For $T < T_-$ — the system is a paramagnetic metallic (PM). For $U_{\rm lc} < U < U_{\rm c}$ and $T_- < T < T_+$, the system is a paramagnetic insulator (the lattice of fluctuating spins $S = 1/2$). For $T > T_+$, the re-entrant metallic behavior is observed (a crossover transition). Such a sequence is indeed observed for V_2O_3 doped with Cr [41] and for liquid ^{3}He. The most important factor is the sequence of transformations between localized and itinerant (liquid) states of the valence electrons as a function of temperature and interaction, as shown schematically in Fig. 6 (a).

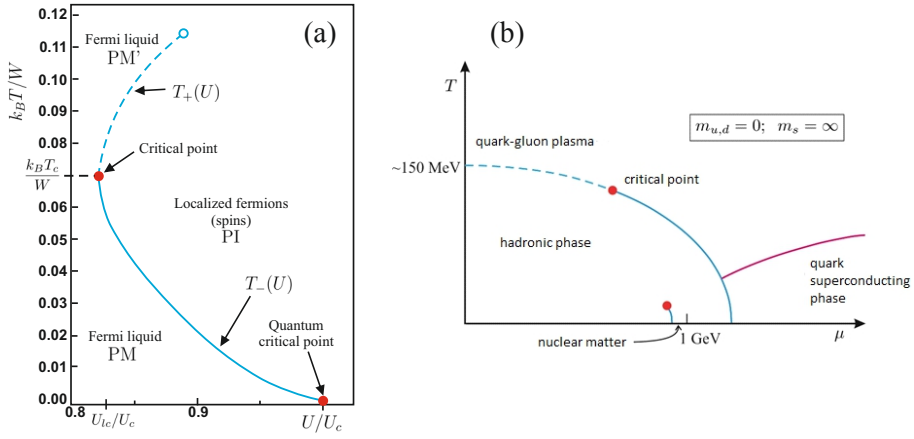

Fig. 6. (a) Phase diagram at $T \neq 0$ for almost localized fermions on the plane temperature T *versus* relative interaction magnitude $U/U_{\rm c}$. Note the presence of two critical points: classical at $T = T_{\rm c}$ and quantum at $T = 0$. This phase diagram does not include the magnetic phases (see below [38]); (b) an analogical phase diagram for the nuclear matter [39]. The dashed lines represent extrapolations to high-temperature regime.

The physical reason for switching between the states M and I is provided in Fig. 7. Namely, at temperature close to $T = 0$, the entropy of disordered localized moments is large ($+k_{\rm B}\ln 2$ per carrier), whereas for the Fermi liquid, it increases linearly with T from zero. Hence, at $T = T_-$, the entropy part of the free energy for localized particles outweighs that of the Fermi

liquid, even though at $T = 0$, the opposite is true. However, as the temperature rises, the Fermi-liquid entropy grows and asymptotically approaches the value $2k_{\mathrm{B}} \ln 2$ per carrier in the high-temperature limit. The detailed shape of the phase boundary is determined by the interplay between the competing energy and entropy contributions. In summary, the continuous evolution of the system at $T = 0$ in approaching U_{c} from below should be contrasted with the discontinuous nature of the transformation for $T > 0$. Thus, the point $U = U_{\mathrm{c}}$ for $T = 0$ is indeed a quantum critical point, at least within this analysis in which $d^2 = \langle n_{i\uparrow} n_{i\downarrow} \rangle$ plays the role of the order parameter in the expression for the Ginzburg–Landau functional for almost localized fermions.

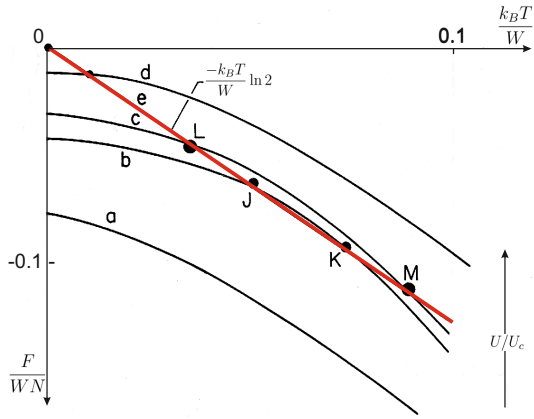

Fig. 7. Temperature dependence of the free energy per particle (F/WN) in Fermi-liquid states (parabolas a–d), and in the Mott–Hubbard localized state (straight line e). The crossing points LM and JK represent, respectively, M $\rightarrow$ I and I $\rightarrow$ M' transitions.

At the end, we would like to quote our results on metal–insulator transition including simultaneous presence of antiferromagnetism which with the increasing interaction magnitude evolves from band (Slater-type AFS) to localized spin (Mott, AFI) antiferromagnetism. The part of the phase diagram depicted in Fig. 6 (a) appears only above the Néel temperature, where the antiferromagnetic states (AFS, AFI) cease to exist, here, in a discontinuous manner. The situation is shown in Fig. 8. In the inset, we quote the experimental results obtained for $(\mathrm{V}_{1-x}\mathrm{Cr}_x)_2\mathrm{O}_3$, with the x as the horizontal x-axis. The agreement is qualitatively good.

The presence of the proposed classical critical point (CP) in Figs. 6 (a) and 8 have been also beautifully confirmed much later [42]. It has a mean-field character, exactly the type predicted by our mean-field-like approach [32, 38, 43], which represented the first realistic attempt to extend

theory of metal–insulator transition of the Mott–Hubbard type at $T > 0$. Our results were confirmed much later [44] within the dynamic mean-field approach.

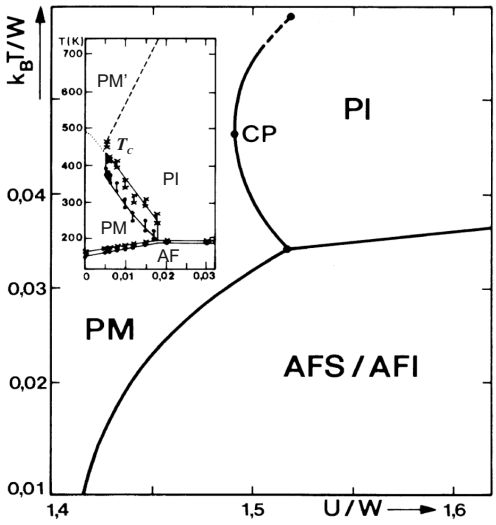

Fig. 8. Phase diagram of the type presented in Fig. 5, with inclusion of antiferromagnetic Slater (AFS) and Mott (AFI) phases. Note that $W = u/2$. Inset: experimentally observed [41] phase diagram on T–x plane for $(V_{1-x}Cr_x)_2O_3$. After Ref. [38].

3. Universal superconductivity: Real-space pairing and selected physical properties

3.1. High-temperature superconductivity: A brief overview

The appearance of high-temperature (high-T_c) superconductivity [45] opened up a completely new area of research for strongly correlated systems. The first of them is that the paired state evolves by doping from the antiferromagnetic Mott-insulating state. The exemplary simplest phase diagram for $La_{2-x}Sr_xCuO_4$ is shown in Fig. 9. It is commonly accepted that by the Sr substitution for La one creates a hole (missing electron). This hole is created in the $Cu^{2+}O^{2-}$ planar configuration of this compound, as schematically illustrated in Fig. 10, which is sandwiched by the insulating La(Sr)O planes. The system can be modeled to a good degree by a periodic arrangement of the CuO_2 planes well-separated by the insulating La(Sr)O planes. In effect, the system at optimal doping $x = x_{opt} \simeq 0.2$ can be regarded as a two-dimensional metal, *i.e.*, metallic state with linear in T in plane resistivity $\rho_{\parallel}$ in the normal state and quasi-exponentional (semiconducting-like) behavior of $\rho_{\perp}$ when measured across the planes. The resistivity ratio

$\rho_\perp/\rho_\parallel$ can reach the value of 10^5, so the system can indeed be regarded as a *two-dimensional* metal. The surprise comes when the system is cooled to the superconducting transition temperature $T_c \simeq 36\,\mathrm{K}$, where the truly *three-dimensional* paired state sets in. Thus, at T_c we have a *dimensional crossover*, a rather exceptional than typical critical behavior in a system with a continuous phase transition. Nonetheless, one can also observe that this transition can take place in strictly two-dimensional layers with the value of $T_c \simeq 100\mathrm{K}$, so assuming a strict two-dimensionality for modeling purpose looks realistic and is practically universally accepted (see below).

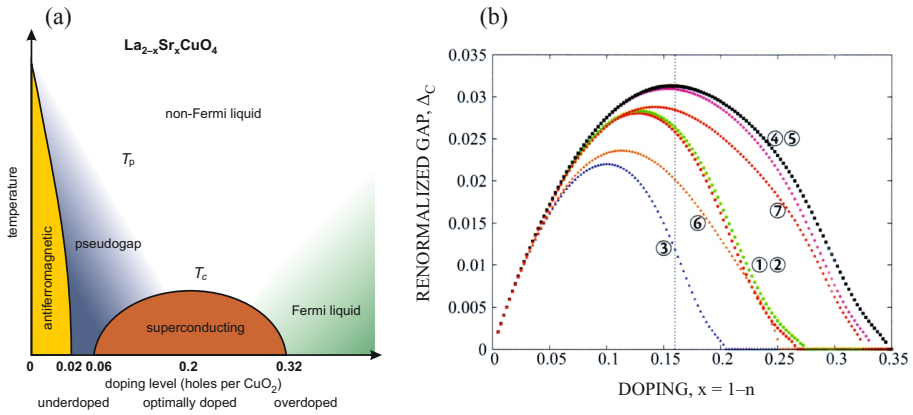

Fig. 9. (a) Schematic phase diagram on the temperature doping (x) plane for $La_{2-x}Sr_xCuO_4$. (b) The same as (a) but on the superconducting gap-doping plane calculated within SGA [46] in t–J model. For explanation, see the main text. The different curves in (b) correspond to a different model parametrization.

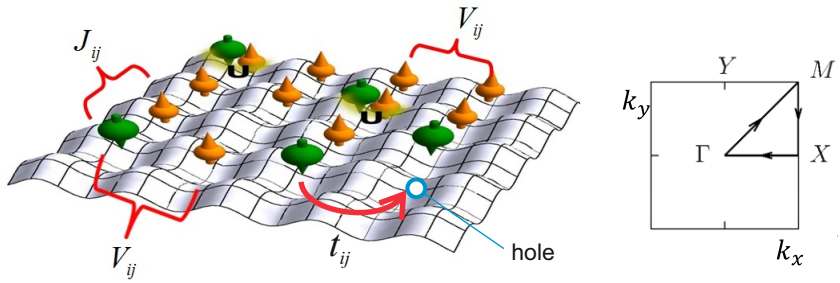

Fig. 10. Illustration of single-band dynamics of correlated electrons in two dimensions with the parameters defined in the main text. On the right: the Brillouin zone with the high-symmetry points marked. The line Γ–M is called the nodal line for the case of d-wave superconductivity, whereas the Γ–X and Γ–Y directions are antinodal ones.

The third surprising feature is the appearance of a well-defined *pseudogap* temperature $T_{\rm pg}$, which appears at temperature well above $T_{\rm c}$, particularly in the underdoped region $x < x_{\rm opt}$. In Fig. 11, we exhibit a comparison between the values of $T_{\rm c}$ and $T_{\rm pg}$ *versus* x (taken from Ref. [47]). In reality, the phase diagram is more complicated than that presented in either Fig. 9 or Fig. 11, as is discussed below.

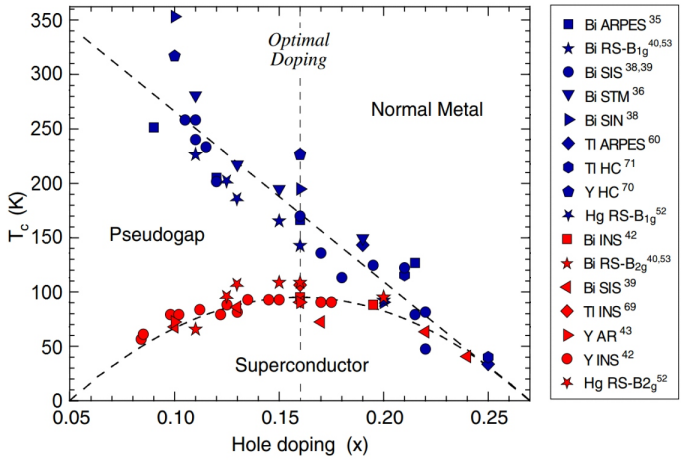

Fig. 11. The hole-doping dependence of the transition temperature $T_{\rm c}$ (lower set of points on the left) and pseudogap characteristic energy (upper set of points on the right). The appearance of the pseudogap is a characteristic novel property for unconventional superconductors (adopted on the basis of Ref. [47]).

3.2. Theoretical modeling of high-$T_{\rm c}$ superconductors as correlated two-dimensional systems: t–J model

3.2.1. The pairing Hamiltonian with real-space pairing

We turn next to the theoretical modeling of strongly correlated metallic state, in which I have been involved personally. The theoretical modeling of the so-called correlated narrow-band systems started with the works of Anderson [6, 7] on antiferromagnetic kinetic exchange in which the Hubbard model was intuitively introduced for the first time.

This Hamiltonian in the strongly correlated limit, $U \gg |t_{ij}|$, and in the half-filled band configuration leads to the antiferromagnetic Heisenberg spin–spin interaction with the exchange integral $J_{ij} = 4t_{ij}^2/U$. The non-half filling case ($n \neq 1$), the Hubbard Hamiltonian has been analyzed for the first time by the author and the results were published in cooperation with

his colleagues [8–10]. The effective Hamiltonian is then

$$\tilde{\mathcal{H}} = P_1 \left\{ \sum_{ij\sigma}{}' t_{ij}\, \hat{b}^\dagger_{i\sigma}\, \hat{b}_{j\sigma} + \frac{1}{2} \sum_{ij}{}' J_{ij} \left(\boldsymbol{S}_i \cdot \boldsymbol{S}_j - \frac{1}{4} \nu_i\, \nu_j \right) + \begin{pmatrix} \text{three-site} \\ \text{terms} \end{pmatrix} \right\} P_1 \,, \tag{17}$$

where now $\hat{b}^\dagger_{i\sigma} \equiv \hat{a}^\dagger_{i\sigma}(1 - \hat{n}^\dagger_{i\bar{\sigma}})$, $\hat{b}_{i\sigma} \equiv (\hat{b}^\dagger_{i\sigma})^\dagger$, $\hat{\boldsymbol{S}}_i$ is the spin operator in the fermionic representation and $\nu_i \equiv \sum_\sigma \hat{n}_{i\sigma}(1 - \hat{n}_{i\bar{\sigma}})$. The operators acting in the occupation number (Fock) space are projected with the operator P_1 in such a manner that *all* site double occupancies are removed (to reduce the Coulomb energy $U \sum_i \langle \hat{n}_{i\uparrow}\, \hat{n}_{i\downarrow} \rangle$) and replaced with *the low-energy virtual hopping processes* on the scale $J_{ij} \ll U$. In the Mott insulating limit, we have a drastic reduction of the occupancy (note that $P_1 \equiv \prod_i (1 - \hat{n}_{i\uparrow}\, \hat{n}_{i\downarrow})$) to the single occupancies at each site, *i.e.*, $\hat{\nu}_i = \sum_\sigma P_1 \langle \hat{n}_{i\sigma} + \hat{n}_{i\bar{\sigma}} \rangle P_1 = 1$; then (17) reduces to the Anderson–Heisenberg form, as it should be. Hamiltonian (17) represents the first step of the modeling procedure.

The second nontrivial step starts from the ingenious quantitative observation by Anderson [2, 48] that antiferromagnetic arrangement of neighboring spins may be viewed as the precursor of the spin-singlet pairing on neighboring sites in the corresponding Wannier states.

After I learned about such a possibility [48, 49] I have introduced [12] the local-singlet pairing operators, since the full exchange term (the $\hat{\boldsymbol{S}}_i \cdot \hat{\boldsymbol{S}}_j - \frac{1}{4} \hat{\nu}_i \hat{\nu}_j$) can be rigorously rewritten in the form of

$$\hat{B}^\dagger_{ij} \equiv \frac{1}{\sqrt{2}} \left(\hat{b}^\dagger_{i\uparrow}\, \hat{b}^\dagger_{j\downarrow} - \hat{b}^\dagger_{i\downarrow}\, \hat{b}^\dagger_{j\uparrow} \right) ; \qquad \hat{B}_{ij} \equiv \left(\hat{B}^\dagger_{ij} \right)^\dagger , \tag{18}$$

so that

$$J_{ij} \left(\hat{\boldsymbol{S}}_i \cdot \hat{\boldsymbol{S}}_j - \frac{1}{4} \hat{\nu}_i\, \hat{\nu}_j \right) = -J_{ij}\, \hat{B}^\dagger_{ij}\, \hat{B}_{ij} \,. \tag{19}$$

As a result, the exchange energy is lowered by the creation of local singlets $|ij, \uparrow\downarrow\rangle \equiv \frac{1}{\sqrt{2}} (|i\uparrow\rangle |j\downarrow\rangle - |i\downarrow\rangle |j\uparrow\rangle)$, not necessarily the classical Néel-type antiferromagnetic state, particularly since the system is two-dimensional and particles have spin $S = 1/2$.

The extra bonuses coming from such a representation are three. *First*, the effective Hamiltonian (17) can be rewritten in a more closed form, *i.e.*,

$$\tilde{\mathcal{H}} = P_1 \left\{ \sum_{ij\sigma}{}' t_{ij}\, \hat{b}^\dagger_{i\sigma}\, \hat{b}_{j\sigma} - \sum_{ijk}{}' \frac{2 t_{ij}\, t_{jk}}{U} \hat{B}^\dagger_{ij}\, \hat{B}_{kj} \right\} P_1 \,. \tag{20}$$

Second, the pairing is indeed of local but *intersite* in nature, since it is easy to show that $\hat{B}^{\dagger}_{ii} \equiv 0$. This is because

$$\hat{B}^{\dagger}_{ij} = \frac{1}{\sqrt{2}} \left[\hat{a}^{\dagger}_{i\uparrow} \left(1 - \hat{n}^{\dagger}_{i\downarrow}\right) \hat{a}^{\dagger}_{j\downarrow} \left(1 - \hat{n}^{\dagger}_{j\downarrow}\right) - \hat{a}^{\dagger}_{i\downarrow} \left(1 - \hat{n}^{\dagger}_{i\uparrow}\right) \hat{a}^{\dagger}_{j\uparrow} \left(1 - \hat{n}^{\dagger}_{j\downarrow}\right) \right] , \tag{21}$$

and for $i = j$,

$$\hat{a}^{\dagger}_{i\sigma} \left(1 - \hat{n}_{i\bar{\sigma}}\right) \hat{a}^{\dagger}_{i\bar{\sigma}} \left(1 - \hat{n}_{i\sigma}\right) = \hat{a}^{\dagger}_{i\sigma}\, \hat{a}_{i\bar{\sigma}}\, \hat{a}^{\dagger}_{i\bar{\sigma}}\, \hat{a}^{\dagger}_{i\bar{\sigma}} \ldots \equiv 0 \,, \quad \textit{etc.} \tag{22}$$

Note that identity (22) does not appear when one uses (wrongly!) *the unprojected* pairing operators, a common omission.

Nonetheless, one can think of the corresponding order parameter in the form of anomalous average $\langle \hat{B}^{\dagger}_{ij} \rangle$. In that situation, its space Fourier transform can play a role of the superconducting gap, at least in *Renormalized Mean-Field Theory* (RMFT). Explicitly, we define the gap parameter in the translationally invariant case as

$$\Delta_{\boldsymbol{k}} \equiv \left\langle \hat{B}^{\dagger}_{\boldsymbol{k},-\boldsymbol{k}} \right\rangle = \frac{1}{N} \sum_{\boldsymbol{R}_{ij}} \mathrm{e}^{i\boldsymbol{k}\cdot\boldsymbol{R}_{ij}} \left\langle \hat{B}^{\dagger}_{ij} \right\rangle \simeq \left\langle \hat{b}^{\dagger}_{\boldsymbol{k}\uparrow}\, \hat{b}^{\dagger}_{-\boldsymbol{k}\downarrow} \right\rangle , \tag{23}$$

where $\boldsymbol{R}_{ij} \equiv \boldsymbol{R}_j - \boldsymbol{R}_i$. *Third*, from (23) it follows that the superconducting gap $\Delta_{\boldsymbol{k}}$ has the property

$$\sum_{\boldsymbol{k}} \Delta_{\boldsymbol{k}} \equiv \sum_{\boldsymbol{k}} \left\langle \hat{B}^{\dagger}_{\boldsymbol{k},-\boldsymbol{k}} \right\rangle = 0 \,, \tag{24}$$

i.e., the value of the superconducting gap, when averaged over the Brillouin zone, is zero. On the other hand, since

$$\left\langle \hat{B}^{\dagger}_{ij} \right\rangle = \frac{1}{\sqrt{2}} \left(\left\langle \hat{b}^{\dagger}_{i\uparrow}\, \hat{b}^{\dagger}_{j\downarrow} \right\rangle - \left\langle \hat{b}^{\dagger}_{i\downarrow}\, \hat{b}^{\dagger}_{j\uparrow} \right\rangle \right) , \tag{25}$$

from the translational symmetry $i \leftrightarrow j$, we have

$$\left\langle \hat{B}^{\dagger}_{ij} \right\rangle = \sqrt{2} \left\langle \hat{b}^{\dagger}_{i\uparrow}\, \hat{b}^{\dagger}_{j\downarrow} \right\rangle , \tag{26}$$

i.e., the prospective order parameter has a structure similar to the corresponding one, $\langle \hat{a}^{\dagger}_{\boldsymbol{k}\uparrow}\, \hat{a}^{\dagger}_{-\boldsymbol{k}\downarrow} \rangle$ in the $\boldsymbol{k}$-space within the Bardeen, Cooper, Schrieffer (BCS) theory.

Property (24) tells us that the gap cannot have the ordinary isotropic (s-wave) structure, *i.e.*, $\Delta_{\boldsymbol{k}} \neq \Delta$. Therefore, the simplest explicitly $\boldsymbol{k}$-dependent representations are those of either extended s-wave or d-wave type, *i.e.*,

$$\Delta_{\boldsymbol{k}} = \Delta \left[\cos\left(k_x a\right) \pm \cos\left(k_y a\right) \right] , \tag{27}$$

where in the subsequent analysis we take $k_x a \equiv k_x$ and $k_y a \equiv k_y$. Those two types fulfill relation (24). In addition, form (27) respects the four-fold symmetry in $\boldsymbol{k}$-space. Nevertheless, there is an essential difference between the two forms of (27). Namely, only the d-wave solution has four nodal (zero-gap) lines defined as $k_y = \pm k_x$. This theoretical prediction (see, *e.g.*, [49]) has been confirmed in numerous experiments and is practically universally accepted.

The three essential features: the t–J model, real-space pairing expressed through the role of the average $\langle \hat{B}_{ij}^{\dagger} \rangle$, and the d-wave form of the gap (minus sign in (27)) compose *a canonical model* of the strong-correlation version of the theory of high-$T_{\rm c}$ superconductivity in the cuprates. The main difficulty is to deal with the projected fermion operators $\hat{b}_{i\sigma}$ (and $\hat{b}_{i\sigma}^{\dagger}$) and the corresponding projected pairing operators (18).

Model (20) can be extended to the most general single-band form, but this is not the subject of interest here (for the most general form of t–J Hamiltonian, see [50]). Instead, in the next section, we reformulate the model to the form which does not require the projection P_1, as well as includes implicitly the role of oxygen anions in the effective exchange part (via superexchange [51]).

3.3. t–J–U–V model as extension of t–J model

To avoid the use of projected Fermi operators, we have proposed [51–53] modification of the original t–J model (17) to the following form:

$$\tilde{\mathcal{H}} = \sum_{ij\sigma}{}' t_{ij}\, \hat{a}_{i\sigma}^{\dagger}\, \hat{a}_{j\sigma} + \frac{1}{2}\sum_{ij}{}' J_{ij}\, \hat{\boldsymbol{S}}_i \cdot \hat{\boldsymbol{S}}_j + U \sum_i \hat{n}_{i\uparrow}\, \hat{n}_{i\downarrow} + \frac{1}{2}\sum_{ij}{}' V_{ij}\, n_i\, n_j\,, \quad (28)$$

where the last term represents the intersite direct Coulomb interaction. At first look, it may seem that the second term should replace the third term, as we argued above. However, in the present formulation of the t–J model by J_{ij} we understand now the superexchange between Cu^{2+} ions via oxygen anions, whereas the Hubbard term ($\sim U$) concerns the repulsive intra-atomic interaction for the electrons on the $3d_{x^2-y^2}$ orbital of Cu ions. Additionally, the double occupancies are projected out if $|t_{ij}| \ll U$, as before. However, in the realistic situation for the cuprates, the effective nearest-neighbor hopping integral is $t \approx -0.3$ eV, whereas $U \simeq 8$–10 eV. In effect, the value of kinetic exchange is $4t^2/U \sim 10^2$ K, far too small when compared to the experimental value $J_{ij} \sim 1500\,\mathrm{K} \simeq 0.13$ eV. In further analysis here, we mention only marginally about the last term $\sim V_{ij}$, *i.e.*, discuss mainly the t–J–U model.

The reason why we have introduced first the t–J model is due to the circumstance that it still constitutes the fundamental basis for analysis of high-T_c superconductivity. We have realized only recently that if we want to keep the above realistic values for t and U, then the bare bandwidth of the effective narrow band is $W \simeq 2.5$–3 eV, so even if U parameter is to be taken as that for Cu^{2+} $d_{x^2-y^2}$ states, (8–10 eV), then we do not have, strictly speaking, the condition of strong correlations ($W \ll U$) fulfilled. In effect, the starting point (28) may be a better choice, particularly if we want to keep the parameter values as set above. Furthermore, the effect of remaining (ligand) orbitals is included implicitly via the exchange term.

3.4. Results for t–J–U model and comparison to experiment for the cuprates

In this subsection, we discuss our results obtained within our original **D**iagramatic **E**xpansion for the **G**utzwiller **W**ave **F**unction (DE-GWF) method elaborated formally in series of papers [51–61]. This method was formulated first for the normal and magnetic states [62–64] and, subsequently, extended to the analysis of unconventional (real-space) paired systems such as high-T_c cuprates [51–61], heavy fermions [65–67], and twisted bilayer graphene [68]. Here, we provide details only for the high-T_c systems. Before going into detailed discussion, we should mention that the DE-GWF method represents a natural extension of the **R**enormalized **M**ean-**F**ield **T**heory (RMFT) in its statistically consistent (SGA) form. Such an extension allowed us for a semiquantitative (in some instances *fully quantitative*) description of selected properties, as elaborated below.

3.4.1. Outline of DE-GWF approach

As discussed above, the general philosophy is to extend the original Gutzwiller approach formulated originally to describe normal and magnetic correlated states [62–64] to the form applicable for description of unconventional superconductivity. For this purpose, we define the correlated many-particle wave function $|\Psi_G\rangle$ with the Ansatz

$$|\Psi_G\rangle = \hat{P}|\Psi_0\rangle\,, \tag{29}$$

where $\hat{P}$ is the properly chosen Guzwiller (non-unitary) projection operator and $|\Psi_0\rangle$ is wave function of corresponding uncorrelated state. The operator $\hat{P}$ has a different form from the original Gutzwiller wave function (*cf.* Büneman *et al.* [62]), but preserves basic properties of the original formulation. Parenthetically, this operator has been selected to allow for a systematic diagrammatic expansion in *real space* (with the corresponding Wick theorem

preserved, *etc.*). The function $|\Psi_0\rangle$ is selected by a self-consistent procedure outlined below; this last selection marks a second departure from the original approach. However, relation (29) is of the original Gutzwiller character, so $|\Psi_{\rm G}\rangle$ can be called Gutzwiller-type wave function (in brief, Gutzwiller WF).

Next, we decompose the total projection into product of site–site components, *i.e.*,

$$P = \prod_i \hat{P} = \prod_i \sum_{\Gamma} \lambda_{i,\Gamma} |\Gamma\rangle_{ii}\langle\Gamma| \,, \tag{30}$$

with variational parameters $\{\lambda_{i,\Gamma}\}$ corresponding to site i occupancies $|\emptyset\rangle_i$, $|\uparrow\rangle_i$, $|\downarrow\rangle_i$ and $|\uparrow\downarrow\rangle_i$: empty, single with spin $\sigma =\uparrow$ or $\downarrow$, or double $\uparrow\downarrow$ occupancies at site i, respectively. Our purpose is to calculate ground-state energy

$$\langle\mathcal{H}\rangle_{\rm G} = \frac{\langle\Psi_{\rm G}|\hat{\mathcal{H}}|\Psi_{\rm G}\rangle}{\langle\Psi_{\rm G}|\Psi_{\rm G}\rangle} = \frac{\langle\Psi_0|\hat{P}\hat{\mathcal{H}}\hat{P}|\Psi_0\rangle}{\langle\Psi_0|\hat{P}^2|\Psi_0\rangle} \,. \tag{31}$$

Now, the trick is to introduce the following representation of the projection operator in a translationally invariant system [62–64]:

$$\hat{P}_i^2 \equiv 1 + x\, \hat{d}_i^{HF} \,, \tag{32}$$

where $\hat{d}_i^{HF} \equiv \hat{n}_{i\uparrow}^{HF}\, \hat{n}_{i\downarrow}^{HF}$, with $\hat{n}_{i\sigma}^{HF} \equiv \hat{n}_{i\sigma} - n_0$, with $n_0 \equiv \langle\Psi_0|\hat{n}_{i\sigma}|\Psi_0\rangle$. Using the normalization condition of the local basis, *i.e.*, ${}_i\langle\Gamma|\Gamma\rangle_i = \delta_{\Gamma\Gamma}$, we can express all the $\{\lambda_{i\Gamma}\}$ parameters via x and hence have just a single variational parameter characterizing $|\Psi_{\rm G}\rangle$ for translationally invariant states.

Two methodological remarks are to be made at this point. First, although operator (30) is a product of single-site operators, the total (multi-site) averages in (31) will still contain intersite products of the local operators, *i.e.*, contain *intersite correlations*. Nevertheless, since the operators $\langle\hat{P}\hat{\mathcal{H}}\hat{P}\rangle_{\rm G}$ and $\langle\hat{P}^2\rangle_{\rm G}$ contain uncorrelated wave function, the multi-site correlation functions may be decomposed into possible pair-site averages $\langle\hat{a}_{i\sigma}^\dagger\hat{a}_{i\sigma}\rangle_0$, $\langle\hat{a}_{i\sigma}^\dagger\hat{a}_{j\sigma'}^\dagger\rangle_0$, *etc.*, which can be calculated self-consistently (subscript 0 means they are evaluated in the uncorrelated state). In the lowest order, one can recover the Gutzwiller-type (SGA) approximation, *e.g.*, $\langle\hat{a}_{i\sigma}^\dagger\hat{a}_{j\sigma}\rangle_{\rm G} \equiv q\langle\hat{a}_{i\sigma}^\dagger\hat{a}_{j\sigma}\rangle_0$, *etc.* Such a procedure provides a fast method of obtaining results, but provides also the reason why the Gutzwiller (GA) and Gutzwiller-type (SGA) approximations cannot yield a stable paired (superconducting) state in a purely repulsive Hubbard model. In this respect, the t–J and t–J–U models provide nontrivial results already in the lowest order. Finally, we introduce the so-called *effective Hamiltonian method* to determine $|\Psi_0\rangle$. First, we note that apart from variational parameter x, we have to determine self-consistently also the averages $\langle\hat{a}_{i\sigma}^\dagger\hat{a}_{j\sigma}\rangle_0$

and $\langle \hat{a}^{\dagger}_{i\uparrow} \hat{a}_{j\downarrow} \rangle_0$. This can be carried out by imposing the condition for minimum with respect to $|\Psi_0\rangle$ of the functional with the Lagrange multiplier $\langle \mathcal{H} \rangle_{\rm G} \equiv \langle \Psi_{\rm G} | \hat{\mathcal{H}} | \Psi_{\rm G} \rangle - \lambda (\langle \Psi_0 | \Psi_0 \rangle - 1)$, *i.e.*, by imposing formally the necessary condition

$$\frac{\delta \left[\mathcal{F} - \lambda \left(\langle \Psi_0 | \Psi_0 \rangle - 1 \right) \right]}{\delta \langle \Psi_0 |} = 0 \,, \tag{33}$$

where $\mathcal{F} \equiv \langle \mathcal{H}_{\rm G} \rangle - 2\mu_{\rm G}\, n_{\rm G}\, N$, N is the number of sites and $n_{\rm G}$ is the occupancy per site in the $|\Psi_{\rm G}\rangle$ state. In effect, this condition can be brought to the form [54] of diagonalizing the effective single-particle Hamiltonian of the form of

$$\mathcal{H}_0^{\rm eff} \equiv {\sum_{ij\sigma}}' t_{ij}^{\rm eff}\, \hat{a}^{\dagger}_{i\sigma}\, \hat{a}_{j\sigma} + {\sum_{ij}}' \left(\Delta_{ij}^{\rm eff}\, \hat{a}^{\dagger}_{i\uparrow}\, \hat{a}^{\dagger}_{j\downarrow} + \text{h.c.} \right) , \tag{34}$$

with

$$t_{ij}^{\rm eff} \equiv \frac{\delta \mathcal{F}}{\delta P_{ij}} \,, \qquad \Delta_{ij}^{\rm eff} \equiv \frac{\delta \mathcal{F}}{\delta S_{ij}} \,, \tag{35}$$

where $P_{ij} \equiv \langle \hat{a}^{\dagger}_{i\sigma}\, \hat{a}_{j\sigma} \rangle - \delta_{ij} n_0$ and $S_{ij} \equiv \langle \hat{a}^{\dagger}_{i\sigma}\, \hat{a}^{\dagger}_{j\sigma} \rangle_0$. They represent effective hopping and real-space-pairing amplitudes.

The formulation thus reduces to a closed set of equations solved within a self-consistent procedure which, unlike the quantum Monte Carlo approach [69, 70], can be calculated for extended (infinite) systems. This is one of the principal advantages of the method. Our method allows also for an approximate discussion of single-particle properties as complementary to those characterizing the global (macro) correlated state. Concrete physical properties are discussed next. The results are calculated as a function of the range of intersite correlations until they converge to practically asymptotic values (usually, the averages calculated at most up to the fifth coordination spheres are sufficient).

3.4.2. Comparison to experiment

In Fig. 12 (a), (b), we summarize some of our theoretical results obtained within the t–J–U model with the help of DE-GWF method, as well as compare them with experiment (for details see [51]). In Fig. 10 (a), we reproduce the doping dependence of the d-wave superconducting gap magnitude $\Delta_{\rm G}$ in the correlated ground state $|\Psi_{\rm G}\rangle$. We observe the two characteristic points, at which the gap disappears, namely, at the Mott-insulating boundary ($x = 0$) and at the upper critical concentration located at $x \simeq x_{\rm c2} \sim 0.35$ (the individual curves represent different choices of the model parameters, *cf.* [51]). Additionally, the "dome-like" curve exhibits a maximum at the optimal doping, $x = x_{\rm c1} \simeq 0.2$. All these features model the behavior of

$T_c = T_c(x)$ drawn in Fig. 9 (a), except in experiment the holes localize already at $x = 0.05$. Also, the vanishing gap at $x = 0$ is to the instability of correlated metallic phase (represents *the Mot–Hubbard point*). In turn, the same behavior appears deep in the metallic phase (for $x \to x_{c2}$) and is due to the circumstance that the concentration of holes is large enough to break easily the local pairing expressed by $\langle B_{ij}^{\dagger} \rangle$, simply due to the sufficient dilution of carriers by holes. It is a sort of percolation threshold for the proliferation of the pair bonds throughout the whole system [71]. The fact that the pairing vanishes deep inside the metallic state makes this state completely different from BCS state, where the pairs are formed from the momentum states $(\boldsymbol{k}, -\boldsymbol{k})$, which have a spatial extension much larger than the intraatomic distance. Perhaps, even more striking feature of the high-T_c superconductivity has been shown in Fig. 12 (b), where we plot the kinetic energy gain by electrons in the superconducting state with respect to that in the normal (paramagnetic metallic) state. This behavior also differs from that expected in the BCS theory, where the pairs gain in potential energy with respect to the normal state, *i.e.*, it is solely determined by the magnitude of pairing interaction. Here, the pairing interaction is combined with the pair correlated motion. One should note also that other selected properties are reproduced at least semiquantitatively, as reported elsewhere [51].

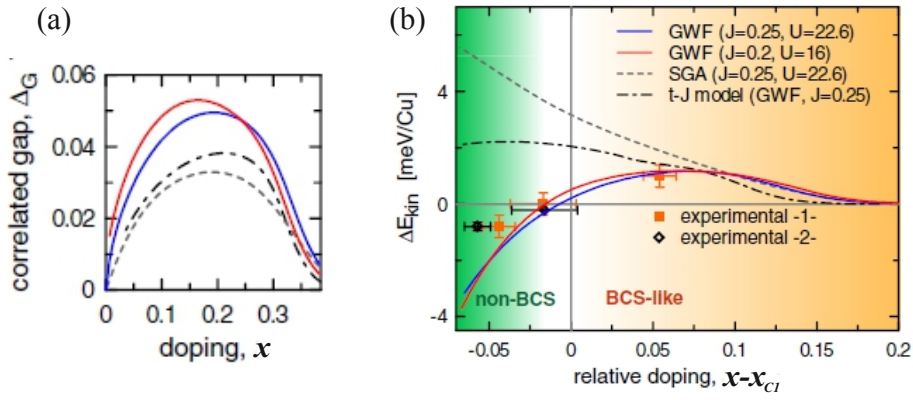

Fig. 12. Pairing d-wave gap in the correlated ground state *versus* x; (b) kinetic energy gain as a function of deviation from the optional doping $x - x_{c1}$. Only the full DE-GWF approach for the t–J–U model reproduces correctly the experimental data (solid lines). Neither SGA approximation in t–J–U model nor t–J model predictions have this property (*cf.* the dashed and dot-dashed curves, respectively). For details, see Ref. [51]. The experimental points are taken from Ref. [72].

Some dynamical properties have also been successfully reproduced by a modified version of our DE-GWF approach, in which the relevant correlation functions have been determined explicitly in the $\boldsymbol{k}$ space. This method has been called k-DE-DWF [73]. The selected results are summarized in Fig. 13 (a), (b). The experimental photoemission spectrum of electron excitation [74] represented in (b) is compared with our results in (a). We see a characteristic kink in the dispersion relation of those correlated particles [75] and the two intervals with an almost-linear dispersion relation of each of them. What is even more intriguing is that the upper part of the excited electrons, very close to the Fermi energy, is almost doping-independent, *i.e.*, of *universal character*. Such a feature is in direct contradiction with what one would export from the band or standard Landau Fermi-liquid theories, where the Fermi velocity (*i.e.*, the slope of the curve $E - E_{\rm F} = v_{\rm F}(k - k_{\rm F})$) should be diminishing with the decreasing carrier concentration [46]. Our present approach successfully reproduces the experimental behavior under the assumption that the Fermi velocity (*i.e.*, that very close to the Fermi level) describes single-electron states of electrons described by $\mathcal{H}_{\rm eff}$ (*cf.* (34)), whereas the part below the kink describes excitations from a well-developed correlated state, *i.e.*, is described by the projected original Hamiltonian $P\hat{\mathcal{H}}P$. Such an assumption can be understood in the following manner. The excitation close to the Fermi surface are of the more ordinary Fermi-liquid-type, since they are the excitations to empty states at and above the Fermi surface; those involve only moderate electron–hole correlations. However they are still essential, since the Fermi velocity $v_{\rm F}$ is x-independent. On the other hand, the excitation from a deeper region below the Fermi surface are of higher energy and require a substantial involvement of higher-energy processes.

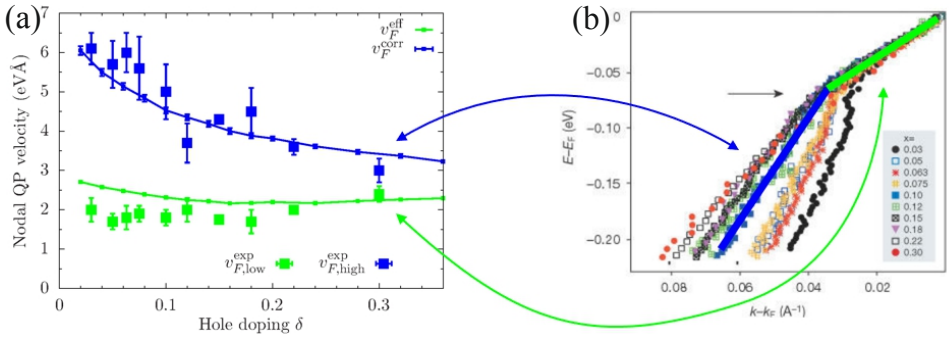

Fig. 13. The photoemission (ARPES) spectrum close to the Fermi level (b) and its decomposition into the linear parts (a), below and above the kink, as shown by the arrows. For discussion, see the main text and Ref. [73].

Associated with the question, that we have both the correlated and effective single-particle states, is that connected with the appearance of the true superconducting gap $\Delta_{\rm G}$ and the pseudogap $\Delta_{\rm pg}$. The former appears as the quantity $\Delta_{\rm G} \sim \langle \hat{a}^{\dagger}_{i\uparrow} \hat{a}^{\dagger}_{j\downarrow} \rangle_{\rm G}$. On the other hand, we have proposed [73] that the *pseudogap* is roughly proportional to the effective gap $\sim \Delta^{\rm eff}_{ij}$. In effect, whereas the ground-state characteristics such as $\Delta_{\rm G}$ and the electron spectrum deep inside the Fermi volume are fully correlated, the universal Fermi velocity, Fermi wave-vector, pseudogap, *etc.* are interpreted as characteristics obtained from the effective single-particle dynamics represented by $\hat{\mathcal{H}}_{\rm eff}$. This interpretation, although in agreement with selected experimental properties, requires thorough further investigation. One must underline that the effective Hamiltonian described the single-particle excitations that correspond to quasiparticle excitations in ALFL, *i.e.*, below the Mott threshold.

4. Outlook

In this paper, we have overviewed briefly the three fundamental properties of correlated systems:

(i) the concept of an *almost localized Fermi liquid* with heavy quasiparticles ($m^*/m_0 \ll 1$) and their specific property — *spin-direction-dependent* effective masses of quasiparticles [16, 17, 19, 29, 32];

(ii) localization–delocalization (*Mott–Hubbard*) transitions which may take the form of either insulator–metal transition for electrons systems [35, 44], insulator–superfluid transition in cold-atom bosonic systems [76] or baryon matter to quark–gluon plasma transition in hadronic condensed matter [39];

(iii) *high-temperature superconductivity* induced by a specific real-space-pairing [2, 12, 51] in which an interplay between the strong repulsive Coulomb interaction and exchange interactions play the dominant role.

Below we summarize briefly each of the items *(i)–(iii)*.

(i)+(ii) Almost localized Fermi liquids and their evolution

The heavy masses appear not only in ALFL near the Mott–Hubbard transition, but also for the case of metallic compounds, for the so-called *heavy-fermion systems*, representing the systems of hybridized, *e.g.*, $4f$ electrons with itinerant (conduction) electrons, the former being at the border of Mott localization. A classic example of such a system is $CeAl_3$ [77] properties of which are presented in Fig. 14. It is fascinating that such systems can be described as ordinary metals with electron masses $m^*/m_0 \sim 10^3$ (m_0 — free electron mass in vacuum). In effect, their Fermi temperature can

be estimated as $T_F \equiv \mu/k_B \sim 10\,K$, *i.e.*, is of the same order of magnitude as that of the liquid ^{3}He, which at ambient pressure is $T_F \simeq 2\,K$. In both the heavy-fermion and liquid-^{3}He systems, we can thus destroy the Fermi-surface structure by a moderate thermal disorder of $T \sim 10\,K$. In effect, the system of such fermions should represent for $T \gg T_F$ an incoherent (classical) gas with the molar entropy approaching gradually the value $2R\ln 2$ for spin 1/2 particles and quenched (zero) orbital moment. This is the regime

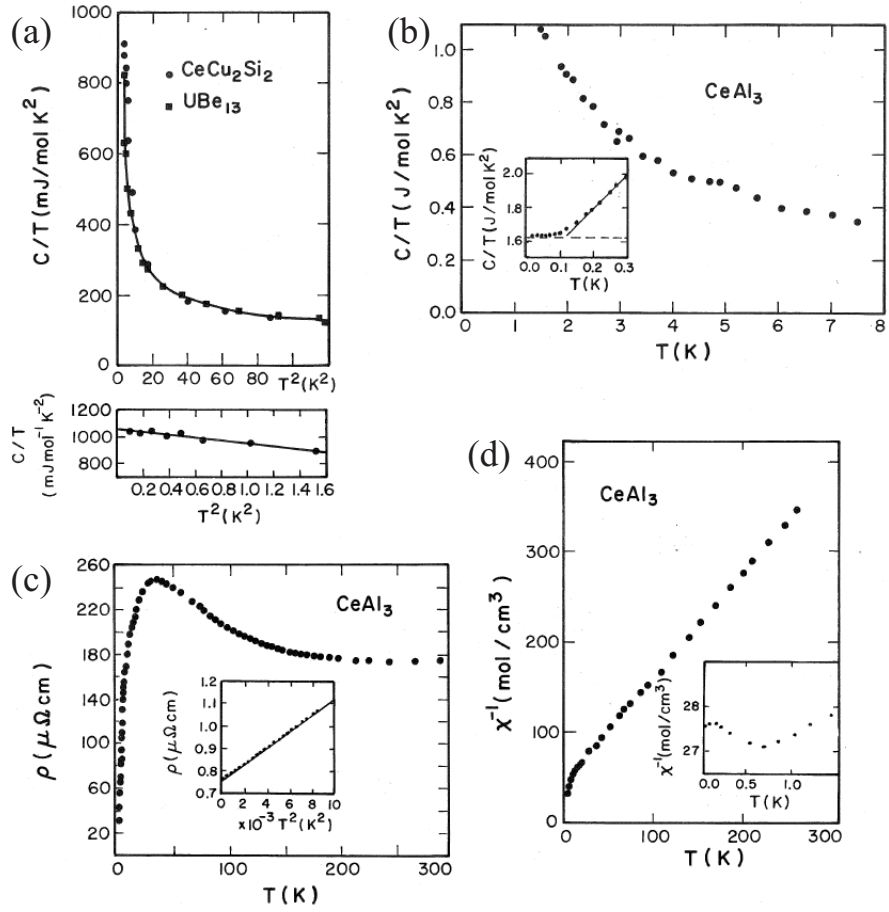

Fig. 14. The fundamental electronic properties of heavy fermions $CeAl_3$ [77], UBe_{13}, and $CeCu_2Si_2$ [78]. The straight lines are guide to the eye. (a) and (b) linear — specific heat coefficient approaching the value $\gamma \gtrsim 1.5/\text{mol K}^2$ as $T \to 0$ for $CeAl_3$ (see also the insets to (a) and (b)); (c) temperature-dependent resistivity approaching the Baber–Ladau–Pomeranchuk $\sim T^2$ dependence as $T \to 0$ (*cf.* the inset); (d) inverse statistic magnetic susceptibility *versus* T (the inset shows the asymptotic Pauli behavior for $T \to 0$). The Curie–Weiss behavior characteristic for localized magnetic moment character for $T \to 0$ is observed.

where the difference between the quasiparticle states in ALFL and the non-interacting fermions arises. Namely, the ALFL quasiparticles describe the correlated state evolving in the heavy-fermion system into a system of localized spins (localized magnetic moments) and the entropy for spin $S = 1/2$ approaches the value $R \ln 2$, *i.e.*, half of the value for the free fermion gas. In Fig. 15, we schematically present such a lattice gas of fermions confined in the localized state within an elementary cell. In the narrow-band system discussed in Section 2, the changeover from itinerant to localized takes the form of discontinuous phase transition. It should be mentioned that the double localized-itinerant nature of f-electron systems is not as sharply defined and still remains debatable. Besides, the quasiparticle behavior of all ALFL systems is related to the simultaneous appearance of robust spin and charge collective fluctuations, not touched upon here [36, 37]. Those quantum fluctuations are particularly important near the quantum phase transitions or either magnetic of delocalization–localization type. For the sake of completeness, in Table I we have summarized simple scaling laws of physical properties due to single-particle (quasiparticle) excitations in ALFL. Note, that all the properties scale with a single renormalization parameter, the inverse mass enhancement factor q. The form of those laws should change if the effects of collective excitations were included.

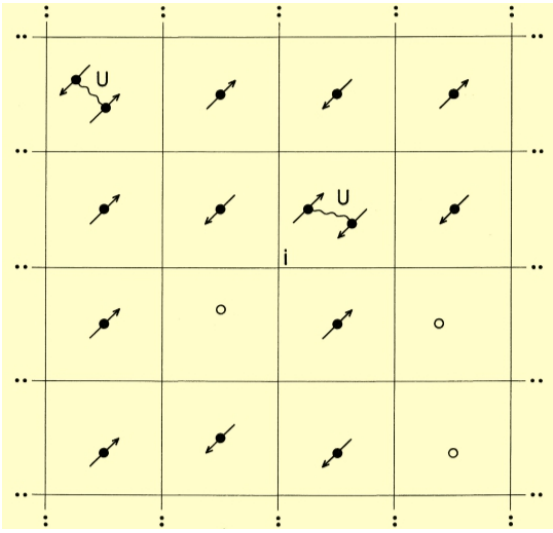

Fig. 15. Lattice gas of fermions of spin 1/2, confined within elementary cells. The parameter $U \gg k_{\mathrm{B}}T$ expresses the repulsive intra-cell interaction (*e.g.*, the Hubbard term) to suppress a double occupancy of the cell by two fermions with opposite spins. This is the principal factor of localization for the average filling of one fermion per cell.

(iii) High-temperature superconductivity

A formal approach developed by our group during the last decade consists of starting from *the statistically-consistent Gutzwiller approximation* (SGA) [46, 52–54] and then generalizing it into a systematic diagrammatic approach for the Gutzwiller wave [51, 54–61]. Very recently, the latter approach has been generalized further to include collective quantum spin and charge excitations (fluctuations) [36]. A detailed review including also the effect of collective excitations is being prepared separately [79]. Here, we have summarized only the main results, particularly those which have a direct comparison to experiment. Let us mention also that our principle aim was (and still is) to develop a *fairly coherence description of overall properties of high-temperature superconductors*, even though it involves utilizing a set of different approximations within the same formal (variational) framework. We discuss briefly only the two features. First of them concerns the variety of phases appearing for high-T_c systems. A schematic plot of such a phase diagram is shown in Fig. 16 (a), (b). The main novel feature is the appearance of charge-density-wave state characterized by temperature T_c, as well as of spin-density-wave state below T_{SDW} (*cf.* Fig. 16 (a), (b)). In connection with this, we have included in our analysis [59] the pair-density-wave appearance and it indeed appears below the optimal doping, in rough accordance with the experiment [80]. Unfortunately, also a small s-wave component of the superconducting gap ($\Delta^s \neq 0$) sets in, a feature which is in disagreement with the persistence of zero gap in the *nodal direction* (*i.e.*, along the $k_x = k_y$ line in the Brillouin zone), a canonical property of the d-wave superconductivity. This difficulty requires a definite clarification.

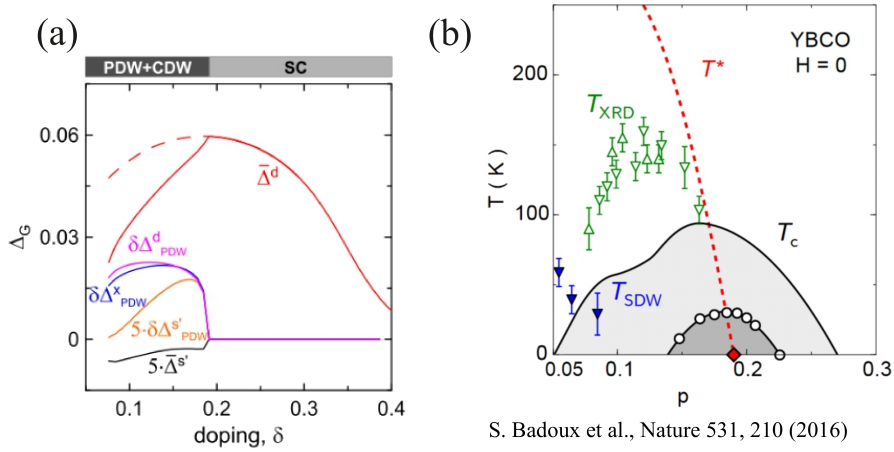

Fig. 16. The phase diagram comprising also various charge-density-wave states: (a) theory and (b) experiment [80]. For details, see Ref. [59].

My interest in correlated systems started in 1976. I thank my Ph.D. Thesis supervisor Prof. Janusz Morkowski from the Polish Academy of Sciences for turning my attention to the subject. Although the idea and the derivation of t–J (and related) models were my own, discussions and cooperation with Koung-An Chao (then at the University of Linköping) and Andrzej M. Oleś were helpful and fruitful. The work on metal–insulator transition was the result of discussions with J.M. Honig (from the Purdue University) and Tom F. Rosebaum (then at the University of Chicago, now at Caltech) of their experimental results. The work on high-$T_{\rm c}$ superconductivity was initiated at the University of Warsaw, with my Ph.D. students (now Professors) Krzysztof Byczuk and Janek Karbowski. This work continued with my tenure at the Jagiellonian University. Here, the Ph.D. students Jakub Jędrak, Jaś Kaczmarczyk, Olga Howczak, M.M. Wysokiński, and M. Abram have been providing the leitmotif for our research during the last 10 years. I thank Dr. Jörg Bünemann for providing us with details of their variational approach. In addition, the definitive work on t–J–U model was carried out with my former Ph.D. student Michał Zegrodnik and Dr. Andrzej Biborski, both from the AGH University of Science and Technology, Kraków. My former students here: Adam Rycerz (now professor), Edward M. Görlich, and Andrzej Kądzielawa were partly instrumental in development of the theory of correlated nanosystems (particularly, in implementation of the EDABI method). Last but not least, I would like to thank Drs. Danuta Goc-Jagło and Maciek Fidrysiak for their cooperation on the current topics associated with the physics of correlated systems, as well as for their technical help. The longtime cooperation with Profs. Włodek Wójcik, Zbigniew Kąkol, and Dr. Robert Podsiadły was important for me for many reasons. Finally, I thank also to Prof. Philip W. Anderson (who passed away recently) for a fruitful correspondence. The work has been financially supported by grant OPUS No. UMO-2018/29/B/ST3/02646 from the National Science Centre, Poland (NCN).

Appendix
Elementary view of localization–delocalization transition

Mott criterion for interaction electron gas

For an ideal nonrelativistic electron gas of spin $S = 1/2$ particles, its kinetic energy (per particle) is

$$\langle T\rangle = \frac{3}{5}\frac{\hbar^2}{2m^*}\left(3\pi^2\frac{N}{V}\right)^{2/3} \sim \rho^{2/3}, \tag{36}$$

where $\rho \equiv N/V$ is the particle density and m^* — its effective mass. On the other hand, we can estimate the static Coulomb interaction per particle as

$$\langle V_{12}\rangle = \frac{e^2}{\kappa r_{12}} = \frac{e^2}{\kappa (V/N)^{1/3}} \;\sim\; \rho^{1/3}\,, \tag{37}$$

where κ is the dielectric constant (here at the border of localization). The fundamental statement is that the instability of the free-electron (delocalized) state can be estimated if the two energies are comparable, *i.e.*, $\langle T\rangle = \langle V_{12}\rangle$. Then, the Mott criterion of localization has the form of

$$a_{\rm B}\,\rho_{\rm c}^{1/3} \;\sim\; 0.2\,, \tag{38}$$

where $a_{\rm B} = \frac{\hbar^2}{m^* e^2}\kappa$ is the effective Bohr radius of $1s$-type atomic state in the medium. Note that if the critical concentration $\rho > \rho_{\rm c}$, the itinerant gas state should be stable as $\langle T\rangle > \langle V_{12}\rangle$, whereas for $\rho < \rho_{\rm c}$, the interaction energy dominates and hence the particles are confined within the cell of radius $a_{\rm c} = \rho_{\rm c}^{-1/3}$. In other words, $a_{\rm B}/a_{\rm c} \sim 1/5$, which means that the effective lattice constant of the frozen spin-1/2 particles is $a \simeq 5a_{\rm B}$. In such a manner, the translational symmetry of the gas state is broken, as the dominant repulsive Coulomb interaction causes the particles distanced from each other as far away as possible. Criterion (38) represents a rudimentary version of the Mott transition. It works surprisingly well for many solid-state systems [1].

Localization–delocalization criterion for confined ultrarelativistic fermions

Suppose we have an ultrarelativistic gas of fermions; for simplicity assume they are of a single color. Then, their Fermi energy is

$$\epsilon_{\rm F} = \hbar c \left(3\pi^2 \rho\right)^{1/3} + \epsilon_0\,, \tag{39}$$

where their kinetic energy of individual particles $\epsilon_k = \hbar c k \equiv cp$ and ϵ_0 is their binding energy in the confined-fermion state. On the other hand, let us assume that we have additional confining pair-particle interaction in the form of

$$\epsilon_{\rm c} = \epsilon_0 + \frac{1}{2}\tilde{k}\,\langle \boldsymbol{r}_i - \boldsymbol{r}_j\rangle^p\,, \tag{40}$$

where $\tilde{k}$ is the interaction parameter. Additionally, the total particle energy is then $\epsilon_0 + 1/2 * (\text{confining potential})$ and p is the exponent depending on the model (usually $p = 1$). In effect, by applying the same condition as above,

i.e., $\langle T \rangle \simeq \epsilon_{\mathrm{F}}/2$, we obtain the critical concentration for the localization–delocalization transition

$$\rho_{\mathrm{c}}^{p+1} = \frac{1}{3\pi^2} \left(\frac{\tilde{k}}{2\hbar c} \right)^3 . \tag{41}$$

Note that the particles are confined in space, but the nature of their quantum states changes at the critical density. For their stability, an external potential is needed first. It is the periodic potential for electrons in solid and the harmonic trapping potential for cold atoms or quarks. On this playground, we have an interplay between the kinetic energy (favoring delocalized states) and their mutual repulsive interaction, which favors the frozen (localized) configuration. Both types of the states can have a confined nature on a macro scale.

REFERENCES

[1] N.F. Mott, «Metal–insulator transitions», *Taylor & Francis*, London 1990.

[2] P.W. Anderson, R.A. Broglia, J.R. Schrieffer (Eds.) «Frontiers and borderlines in many-particle physics», *North-Holland*, Amsterdam 1988, pp. 1–47.

[3] J. Hubbard, «Electron correlations in narrow energy bands», *Proc. R. Soc. (London) A.* **276**, 238 (1963).

[4] J. Spałek, «Correlated fermions: A new paradigm in physics on the example of solid-state physics?», *Eur. J. Phys.* **21**, 511 (2000).

[5] E. Koch, «Exchange mechanisms», in: E. Pavarini, E. Koch, F. Anders, M. Jarrell (Eds.) «Correlated electrons: From models to materials», *North-Holland*, Amsterdam 1988.

[6] P.W. Anderson, «New approach to the theory of superexchange interactions», *Phys. Rev.* **115**, 2 (1959).

[7] P.W. Anderson, «Theory of magnetic exchange interactions: Exchange in insulators and semiconductors», *Solid State Phys.* **14**, 99 (1963).

[8] J. Spałek, A. Oleś, On the kinetic exchange interactions in the Hubbard model, preprint No. SSPJU — 6/76, October 1976, `http://th-www.if.uj.edu.pl/ztms/download/jSpalek/tJmodel.pdf`

[9] J. Spałek, A.M. Oleś, «Ferromagnetism in narrow s-band with inclusion of intersite correlations», *Physica B+C* **86–88**, 375 (1977).

[10] K.A. Chao, J. Spałek, A.M. Oleś, «Kinetic exchange interaction in a narrow S-band», *J. Phys. C: Solid State Phys.* **10**, L271 (1977).

[11] J. Spałek, Habilitation Thesis, Jagiellonian University, 1981.

[12] J. Spałek, «Effect of pair hopping and magnitude of intra-atomic interaction on exchange-mediated superconductivity», *Phys. Rev. B* **37**, 533 (1988).

[13] F.C. Zhang, T.M. Rice, «Effective Hamiltonian for the superconducting Cu oxides», *Phys. Rev. B* **37**, 3759 (1988).

[14] A.E. Ruckenstein, P.J. Hirschfeld, J. Appel, «Mean-field theory of high-T_c superconductivity: The superexchange mechanism», *Phys. Rev. B* **36**, 857 (1987).

[15] J. Hubbard, «Electron correlations in narrow energy bands III. An improved solution», *Proc. R. Soc. (London) A* **281**, 401 (1964).

[16] J. Spałek, P. Gopalan, «Almost-localized electrons in a magnetic field», *Phys. Rev. Lett.* **64**, 2823 (1990).

[17] P. Korbel, J. Spałek, W. Wójcik, M. Acquarone, «Spin-split masses and metamagnetic behavior of almost-localized fermions», *Phys. Rev. B* **52**, R2213 (1995).

[18] I. Sheikin *et al.*, «High magnetic field study of $CePd_2Si_2$», *Phys. Rev. B* **67**, 094420 (2003).

[19] J. Spałek, «Spin-split masses and a critical behavior of almost localized narrow-band and heavy-fermion systems», *Physica B* **378–380**, 654 (2006).

[20] A. McCollam *et al.*, «Anomalous de Haas–van Alphen oscillations in $CeCoIn_5$», *Phys. Rev. Lett.* **94**, 186401 (2005).

[21] A.W. Overhauser, «Effective-mass splitting in a magnetized metal», *Phys. Rev. B* **4**, 3318 (1971).

[22] G. Baym, C. Pethick, «Landau Fermi-liquid theory: Concepts and applications», *Wiley*, 1991.

[23] V. Tripathi, «Landau Fermi liquids and beyond», *CRC Press*, Boca Raton 2018.

[24] J. Spałek, «Fermi liquid behavior and the metal-insulator transition of almost localized electrons: A brief theoretical review and an application to V_2O_3 system», *J. Solid State Chem.* **88**, 70 (1990).

[25] A. Rycerz, Physical properties and quantum phase transitions in strongly correlated electron systems from a combined exact diagonalization *ab initio* approach, Ph.D. Thesis, Jagiellonian University, Kraków, 2003.

[26] J. Spałek, E.M. Görlich, A. Rycerz, R. Zahorbeński, «The combined exact diagonalization–*ab initio* approach and its application to correlated electronic states and Mott–Hubbard localization in nanoscopic systems», *J. Phys.: Condens. Matter* **19**, 255212 (2007).

[27] H.A. Mook, «Momentum distribution of ^{3}He», *Phys. Rev. Lett.* **55**, 2452 (1985).

[28] D.S. Greywall, «^{3}He specific heat and thermometry at millikelvin temperatures», *Phys. Rev. B* **33**, 7520 (1986).

[29] J. Spałek, «Magnetic properties of almost localized fermions revisited: spin dependent masses and quantum critical behavior», *Phys. Status Solidi B* **243**, 78 (2006).

[30] W.F. Brinkman, T.M. Rice, «Application of Gutzwiller's variational method to the metal-insulator transition», *Phys. Rev. B* **2**, 4302 (1970).

[31] J. Spałek, A.M. Oleś, J.M. Honig, «Metal-insulator transition and local moments in a narrow band: A simple thermodynamic theory», *Phys. Rev. B* **28**, 6802 (1983).

[32] J. Spałek, M. Kokowski, J.M. Honig, «Low-temperature properties of an almost-localized Fermi liquid», *Phys. Rev. B* **39**, 4175 (1989).

[33] J. Spałek, «Liquids, theory of: Fermi liquids», in: «Encyclopedia of condensed matter physics», *Elsevier*, 2005, pp. 125–135.

[34] J. Spałek, «Liquids, theory of: Fermi liquids», in: «Reference module in materials science and materials engineering», *Elsevier*, Oxford 2016.

[35] D. Vollhardt, «Normal ^{3}He: An almost localized Fermi liquid», *Rev. Mod. Phys.* **56**, 99 (1984).

[36] M. Fidrysiak, J. Spałek, «Robust spin and charge excitations throughout high-T_c-cuprate phase diagram from incipient Mottness», arXiv:1912.06232 [cond-mat.str-el].

[37] M. Fidrysiak, J. Spałek, «Stable high-temperature paramagnons in a three-dimensional antiferromagnet near quantum criticality: Application to $TlCuCl_3$», *Phys. Rev. B* **95**, 174437 (2017).

[38] J. Spałek, A. Datta, J.M. Honig, «Discontinuous metal-insulator transitions and Fermi-liquid behavior of correlated electrons», *Phys. Rev. Lett.* **59**, 728 (1987).

[39] K. Rajagopal, «Mapping the QCD phase diagram», *Nucl. Phys. A* **661**, 150 (1999).

[40] J. Spałek, W. Wójcik, «Almost localized fermions and Mott–Hubbard transitions at non-zero temperature», in: «Spectroscopy of Mott insulators and correlated metals. Springer Series in Solid-State Sciences, vol. 119», *Springer*, Berlin Heidelberg 1995, pp. 41–65.

[41] H. Kuwamoto, J.M. Honig, J. Appel, «Electrical properties of the $(V_{1-x}Cr_x)_2O_3$ system», *Phys. Rev. B* **22**, 2626 (1980).

[42] P. Limelette *et al.*, «Universality and critical behavior at the Mott transition», *Science* **302**, 89 (2003).

[43] J. Spałek, A. Datta, J.M. Honig, «Thermodynamics of the metal-insulator transition: Discontinuous transitions in the paramagnetic phase», *Phys. Rev. B* **33**, 4891 (1986).

[44] A. Georges, G. Kotliar, W. Krauth, M.J. Rozenberg, «Dynamical mean-field theory of strongly correlated fermion systems and the limit of infinite dimensions», *Rev. Mod. Phys.* **68**, 13 (1996).

[45] J.G. Bednorz, K.A. Müller, «Possible high-T_c superconductivity in the Ba–La–Cu–O system», *Z. Phys. B* **64**, 189 (1986).

[46] J. Jędrak, J. Spałek, «Renormalized mean-field t–J model of high-T_c superconductivity: Comparison to experiment», *Phys. Rev. B* **83**, 104512 (2011).

[47] S. Hüfner, M.A. Hossain, A. Damascelli, G.A. Sawatzky, «Two gaps make a high-temperature superconductor?», *Rep. Prog. Phys.* **71**, 062501 (2008).

[48] P.W. Anderson, «The resonating valence bond state in La_2CuO_4 and superconductivity», *Science* **235**, 1196 (1987).

[49] D.J. Scalapino, «A common thread: The pairing interaction for unconventional superconductors», *Rev. Mod. Phys.* **84**, 1383 (2012).

[50] J. Spałek, A.M. Oleś, K.A. Chao, «Magnetic phases of strongly correlated electrons in a nearly half-filled narrow band», *Phys. Status Solidi B* **108**, 329 (1981).

[51] J. Spałek, M. Zegrodnik, J. Kaczmarczyk, «Universal properties of high-temperature superconductors from real-space pairing: t–J–U model and its quantitative comparison with experiment», *Phys. Rev. B* **95**, 024506 (2017).

[52] M. Abram, J. Kaczmarczyk, J. Jędrak, J. Spałek, «d-wave superconductivity and its coexistence with antiferromagnetism in the t–J–U model: Statistically consistent Gutzwiller approach», *Phys. Rev. B* **88**, 094502 (2013).

[53] M. Abram, M. Zegrodnik, J. Spałek, «Antiferromagnetism, charge density wave, and d-wave superconductivity in the extended t–J–U model: Role of intersite Coulomb interaction and a critical overview of renormalized mean field theory», *J. Phys.: Condens. Matter* **29**, 365602 (2017).

[54] J. Kaczmarczyk, «Comparison of two approaches for the treatment of Gutzwiller variational wave functions», *Phil. Mag.* **95**, 563 (2014).

[55] J. Kaczmarczyk, J. Bünemann, J. Spałek, «High-temperature superconductivity in the two-dimensional t–J model: Gutzwiller wavefunction solution», *New J. Phys.* **16**, 073018 (2014).

[56] J. Kaczmarczyk, J. Spałek, T. Schickling, J. Bünemann, «Superconductivity in the two-dimensional Hubbard model: Gutzwiller wave function solution», *Phys. Rev. B* **88**, 115127 (2013).

[57] M. Zegrodnik, J. Spałek, «Effect of interlayer processes on the superconducting state within the t–J–U model: Full Gutzwiller wave-function solution and relation to experiment», *Phys. Rev. B* **95**, 024507 (2017).

[58] M. Zegrodnik, J. Spałek, «Universal properties of high-temperature superconductors from real-space pairing: Role of correlated hopping and intersite Coulomb interaction within the t–J–U model», *Phys. Rev. B* **96**, 054511 (2017).

[59] M. Zegrodnik, J. Spałek, «Incorporation of charge- and pair-density-wave states into the one-band model of d-wave superconductivity», *Phys. Rev. B* **98**, 155144 (2018).

[60] M. Zegrodnik, J. Spałek, «Stability of the coexistent superconducting-nematic phase under the presence of intersite interactions», *New J. Phys.* **20**, 063015 (2018).

[61] M. Zegrodnik, A. Biborski, M. Fidrysiak, J. Spałek, «Superconductivity in the three-band model of cuprates: Variational wave function study and relation to the single-band case», *Phys. Rev. B* **99**, 104511 (2019).

[62] J. Bünemann, T. Schickling, F. Gebhard, «Variational study of Fermi surface deformations in Hubbard models», *Europhys. Lett.* **98**, 27006 (2012).

[63] J. Bünemann, W. Weber, F. Gebhard, «Multiband Gutzwiller wave functions for general on-site interactions», *Phys. Rev. B* **57**, 6896 (1998).

[64] J. Bünemann, S. Wasner, E.v. Oelsen, G. Seibold, «Exact response functions within the time-dependent Gutzwiller approach», *Phil. Mag.* **95**, 550 (2014).

[65] M.M. Wysokiński, J. Kaczmarczyk, J. Spałek, «Gutzwiller wave-function solution for Anderson lattice model: Emerging universal regimes of heavy quasiparticle states», *Phys. Rev. B* **92**, 125135 (2015).

[66] M.M. Wysokiński, J. Kaczmarczyk, J. Spałek, «Correlation-driven d-wave superconductivity in Anderson lattice model: Two gaps», *Phys. Rev. B* **94**, 024517 (2016).

[67] J. Kaczmarczyk, J. Spałek, «Coexistence of antiferromagnetism and superconductivity within t–J model with strong correlations and nonzero spin polarization», *Phys. Rev. B* **84**, 125140 (2011).

[68] M. Fidrysiak, M. Zegrodnik, J. Spałek, «Unconventional topological superconductivity and phase diagram for an effective two-orbital model as applied to twisted bilayer graphene», *Phys. Rev. B* **98**, 085436 (2018).

[69] M. Randeria, R. Sensarma, N. Trivedi, «Projected wavefunctions and high T_c superconductivity in doped Mott insulators», in: A. Avella, F. Manini (Eds.) «Strongly correlated systems. Springer Series in Solid-State Sciences, vol. 171», *Springer Verlag*, Berlin 2011, pp. 29–64.

[70] F. Becca, S. Sorella, «Quantum Monte Carlo approaches for correlated systems», *Cambridge University Press*, 2017.

[71] J. Spałek, D. Goc-Jagło, «On the strongly correlated quantum matter paradigm: magnetism-superconductivity redux», *Phys. Scr.* **86**, 048301 (2012).

[72] G. Deutscher, A.F. Santander-Syro, N. Bontemps, «Kinetic energy change with doping upon superfluid condensation in high-temperature superconductors», *Phys. Rev. B* **72**, 092504 (2005).

[73] M. Fidrysiak, M. Zegrodnik, J. Spałek, «Realistic estimates of superconducting properties for the cuprates: reciprocal-space diagrammatic expansion combined with variational approach», *J. Phys.: Condens. Matter* **30**, 475602 (2018).

[74] X.J. Zhou *et al.*, «Universal nodal Fermi velocity», *Nature* **423**, 398 (2003).

[75] K. Byczuk *et al.*, «Kinks in the dispersion of strongly correlated electrons», *Nature Phys.* **3**, 168 (2007).

[76] M. Greiner *et al.*, «Quantum phase transition from a superfluid to a Mott insulator in a gas of ultracold atoms», *Nature* **415**, 39 (2002).

[77] K. Andres, J.E. Graebner, H.R. Ott, «$4f$-virtual-bound-state formation in $CeAl_3$ at low temperatures», *Phys. Rev. Lett.* **35**, 1779 (1975).

[78] F. Steglich *et al.*, «Superconductivity in the presence of strong Pauli paramagnetism: $CeCu_2Si_2$», *Phys. Rev. Lett.* **43**, 1892 (1979).

[79] J. Spałek, M. Fidrysiak, M. Zegrodnik, A. Biborski, *Phys. Rep.*, in prepearation.

[80] S. Badoux *et al.*, «Change of carrier density at the pseudogap critical point of a cuprate superconductor», *Nature* **531**, 210 (2016).